

**“Structural and photoluminescence properties of Dy³⁺ ions doped
potassium magnesium molybdate phosphor for lighting devices”**

SUBMITTED IN PARTIAL FULFILLMENT OF THE REQUIREMENTS FOR THE
AWARD OF THE DEGREE
MASTERS OF SCIENCE
IN
PHYSICS

Submitted by:

Yashika Saraswat

2K22/MSCPHY/49

Chitrangi Bhardwaj

2K22/MSCPHY/56

Under the supervision of

Prof. A. S. Rao



DEPARTMENT OF APPLIED PHYSICS

DELHI TECHNOLOGICAL UNIVERSITY

(Formerly Delhi College of Engineering)

Bawana Road, Delhi – 110042

JUNE, 2024

DECLARATION

We hereby certify that the work which is presented in the Major Project-II entitled “: **Structural and photoluminescence properties of Dy³⁺ ions doped potassium magnesium molybdate phosphor for lighting devices**” in fulfilment of the requirement for the award of the Degree of Master of Science in Physics and submitted to Department of Applied Physics, Delhi Technological University, Delhi is an authentic record of our own, carried out during a period from 2023-2024, under the supervision of **Prof. A.S. Rao**, Department of Applied Physics, Delhi Technological University, Delhi.

The matter presented in this thesis has not been submitted by us for the award of any other degree of this or any other Institute/University. The work has been published/accepted/communicated in SCI/SCI expanded/SSCI/Scopus indexed journal or peer reviewed Scopus indexed conference with the following details:

Title of the paper: **Structural and photoluminescence properties of Dy³⁺ ions doped potassium magnesium molybdate phosphor for lighting devices.**

Author names: Yashika Saraswat, Chitrangi Bhardwaj and A.S. Rao Name of Journal: Luminescence (Scopus Indexed)

Status of paper (Accepted/Published/Communicated): Revision Communicated Date of paper

communication: February 15, 2024

Date of paper acceptance:

Have you registered for the conference? Yes

Physics with Application (ICAMNOP).

Title of the paper: **Photoluminescence studies of molybdate phosphor doped with Dy³⁺ ions for w- LEDs.**

Status of paper (Accepted/Published/Communicated): Accepted

Conference Dates with venue: December 20-22, 2023, Delhi Technological University



Yashika Saraswat
Roll No.: 2K22/MSCPHY/49



Chitrangi Bhardwaj
Roll No.:2K22/MSCPHY/56

SUPERVISOR CERTIFICATE

To the best of my knowledge, the above work has not been submitted in part or full for any Degree of Diploma to this University or elsewhere. I further certify that the publication and indexing information given by the students is correct.



Place: Delhi

Prof.

A.S. Rao

Date: 07/06/2024

Department of Applied Physics (DTU)
Supervisor

DELHI TECHNOLOGICAL UNIVERSITY

(FORMERLY Delhi College of
Engineering) Bawana Road,
Delhi-110042

CERTIFICATE

I hereby certify that the project Dissertation titled “**Structural and photoluminescence properties of Dy³⁺ ions doped potassium magnesium molybdate phosphor for lighting devices**” which is submitted by YASHIKA SARAWAT (2K22/MSCPHY/49), CHITRANGI BHARDWAJ (2K22/MSCPHY/56) [Masters in Physics], Delhi Technological University, Delhi in fulfillment of the requirement for the award of the degree of the Master of Physics, is a record of the project work carried out by the students under my supervision. To the best of my knowledge this work has not been submitted in partition or full for any Degree or Diploma to this University or elsewhere.



Place: Delhi

Prof. A. S. Rao

Date: 07/06/2024

SUPERVISOR

ACKNOWLEDGEMENT

We would like to convey our heartfelt thanks to Prof. A.S. Rao, Department of Applied Physics, Delhi Technological University, for allowing us to work under his supervision and for providing us with continual inspiration and unwavering support throughout the project. We'd like to take this occasion to thank our supervisor for his passionate assistance, knowledge, fantastic ideas, useful comments, and consistent support. We are appreciative of the continual assistance and convenience provided by all lab members (Ph.D. scholars), especially Ms. Sheetal Kumari, Dept. of Applied Physics, at every stage of our study. Furthermore, we have been fortunate and thankful to our family and friends for their love, care, as they patiently extended all kinds of assistance to help us complete this duty.



YASHIKA SARASWAT



CHITRANGI BHARDWAJ

Contents

CANDIDATE’S DECLARATION.....	2
CERTIFICATE.....	4
ACKNOWLEDGEMENT.....	5
LIST OF FIGURES	8
LIST OF TABLES	10
LIST OF ABBREVIATIONS	11
Abstract.....	12
CHAPTER 1: INTRODUCTION.....	13
1.1 Phosphor	13
1.2 Host matrix and activator ions.....	15
1.3 White light emitting diodes (w-LEDs).....	16
1.4 Photoluminescence (PL).....	17
1.5 Fluorescence and phosphorescence.....	19
CHAPTER 2: INSTRUMENTATION.....	20
2.1 X-ray diffraction (XRD)	20
2.2 Scanning electron microscope (SEM).....	23
2.3 Fourier infrared transform spectroscopy (FT-IR) Analysis	24

2.4 Diffuse reflectance spectroscopy (DRS)	26
2.5 Photoluminescence spectroscopy	27
CHAPTER 3: EXPERIMENTAL PROCEDURE	28
3.1 Phosphor Preparation: Materials and Method	28
CHAPTER 4: RESULTS AND DISCUSSION.....	29
4.1 Structural and elemental studies	29
4.1.1 XRD Analysis	29
4.1.2 Morphology features	29
4.1.3 FTIR Analysis.....	31
4.1.4 DRS and calculations for optical bandgap	32
4.1.2 Photoluminescence.....	35
4.1.3 Y/B intensity ratio	40
4.1.4 CIE coordinate analysis.....	41
4.1.5 PL Decay Profile Analysis	44
CHAPTER 5: CONCLUSIONS	48
CHAPTER 6: SCOPE OF FUTURE WORK	49
REFERENCES.....	50
PLAGIARISM REPORT	53
ACCEPTANCE PROOF	54
SCOPUS INDEXING PROOF	56

LIST OF FIGURES

Fig.1.1. Phosphor emitting Light

Fig.1.2. Jablonski diagram of fluorescence and phosphorescence processes

Fig.2.1. Apparatus for X-ray Diffraction

Fig.2.2. Schematic representation of Bragg's law

Fig.2.3. Xray Tube

Fig.2.4. Scanning electron microscope (SEM)

Fig.2.5. Parts of an FTIR spectrometer with source, interferometer & detector.

Fig.2.6. Diffuse Reflectance Spectroscopy

Fig.2.7. Apparatus for Photoluminescence Spectroscopy

Fig.3.1. Flow chart of synthesis procedure of KMM:xDy^{3+} phosphors.

Fig.4.1 XRD of undoped and Dy^{3+} doped phosphors compared with JCPDS Card No. 84-0155

Fig.4.1(a): SEM images recorded for $\text{K}_2\text{Mg}_2(\text{MoO}_4)_3: x \text{Dy}^{3+}$ ($x=0, 4$ mol %).

Fig.4.2. EDX image of the $\text{K}_2\text{Mg}_2(\text{MoO}_4)_3: x \text{Dy}^{3+}$ ($x= 4$ mol %).

Fig.4.3. FTIR spectrum of an un-doped $\text{K}_2\text{Mg}_2(\text{MoO}_4)_3$ phosphor.

Fig.4.4. Diffuse reflectance spectra of $\text{K}_2\text{Mg}_2(\text{MoO}_4)_3: x \text{Dy}^{3+}$ ($1.0 \leq x \leq 5.0$, $\Delta x=1.0$ mol %), phosphors.

Fig.4.5. Tauc plots for direct optical band gap calculation.

Fig. 4.6. PL excitation and emission spectra of KMM:xDy^{3+} ($x = 1.0, 2.0, 3.0, 4.0, 5.0$ mol

%) phosphors under 576 nm emission and 387 nm excitation wavelengths respectively.

Fig.4.7 PL emission spectra of Dy³⁺ ions doped K₂Mg₂(MoO₄)₃ phosphors under 387 nm excitation wavelength.

Fig.4.8. Dexter plot between log(1/x) and log(x)

Fig.4.9. Partial energy level diagram and possible cross- relaxation channels of Dy³⁺ ion doped K₂Mg₂(MoO₄)₃ phosphor

Fig.4.10.CIE chromaticity coordinates of Dy³⁺ ions in K₂Mg₂(MoO₄)₃ phosphors

Fig.4.11. PL decay profile of K₂Mg₂(MoO₄)₃: x Dy³⁺ (0.0≤x≤5.0, Δx=1.0 mol %), phosphors under 387nm excitation.

Fig. 4.12. Dependence of photoluminescence decay lifetime on the Dy³⁺ doping concentration based on Auzel's model.

LIST OF TABLES

Table 4.1. CIE coordinates, CCT values of KMM: $x\text{Dy}^{3+}$ ($1.0 \leq x \leq 5.0$, $\Delta x = 1.0$ mol %) under 387 nm excitation wavelength.

Table 4.2. KMM: $x\text{Dy}^{3+}$ ($x = 1.0, 2.0, 4.0, \text{ and } 5.0$ mol%) phosphors photoluminescence decay duration, non-radiative rate, and luminous effectiveness.

LIST OF ABBREVIATIONS

LED	Light Emitting Diode
WLED	White Light Emitting Diode
pc-WLED	Phosphor Converted White Light Emitting Diode
RE	Rare Earth
XRD	X-Ray Diffraction
PL	Photoluminescence
JCPDS	Joint Committee on Powder Diffraction Standards

Abstract:

A series of $\text{K}_2\text{Mg}_2(\text{MoO}_4)_3$ (KMM) phosphors doped with Dy^{3+} ions were synthesized by the solid-state reaction (SSR) method. The crystal structure and photoluminescence (PL) properties were investigated through instrumentation techniques like X-ray diffraction (XRD) and Spectrofluorophotometer. The KMM material is a member of the $\text{P2}_1\text{2}_1\text{2}_1$ space group and has an orthorhombic structure. Based on the diffuse reflectance spectrum (DRS) measurements, the optical bandgap was calculated. The synthesized phosphor material exhibits a 4f transition of Dy^{3+} ions, excited by 387 nm, and the most intense emission peak was observed at 576 nm. Double exponential behaviour was seen in the PL decay spectral profiles taken under an excitation wavelength of 387 nm. The CIE coordinates of the prepared phosphor lie in yellowish white region. We wish to propose Dy^{3+} ions doped KMM phosphor as a viable material for applications in white light emitting diodes (w-LEDs).

CHAPTER 1: INTRODUCTION

1.1 Phosphor

Phosphors have been utilized since the 19th century as a general term for materials that emit light in the absence of light. Each phosphor possesses unique characteristics, including emission colors and the duration of afterglow following excitation cessation. Electroluminescence is the phenomenon wherein phosphors emit light due to electron excitation. These phosphors find application in the production of video displays and workstation monitors. Photoluminescence involves stimulating phosphors using UV, visible, and infrared radiation and is commonly employed in fluorescent lighting for ambient illumination.



Fig. 1.1. Phosphor emitting light

Phosphors can be categorized into different groups based on the criteria used for classification, specifically focusing on chemical phosphors. Inorganic phosphors, in the form of dry powders, are the most prevalent type. Multiple synthetic methods are employed to produce these powder samples. The basic principle involves incorporating an activator ion, commonly a Rare-Earth ion, into a host matrix. RE ions are frequently used as activators in this context. Phosphors consist of composites like oxide, oxynitride, sulfide, selenide, halide, borates, and oxyhalide, which are doped with small quantities of

activator ions. These activator ions can be either rare-earth or transition element ions. The activator ions serve as centers for radiation or light, possessing their own distinct energy levels that can be stimulated or undergo energy transfer.

A phosphor's efficiency is measured by its ability to utilize excitation energy and emit light, as depicted in Fig. 1.1. To minimize afterglow, it is crucial to minimize the time delay between excitation and emission. Energy absorption can take place at the activator ion or elsewhere in the lattice, but it must ultimately be transferred to the radiating core for emission to occur. The absorbed energy can also be dissipated through radiation-free processes, leading to a decrease in quantum efficiency. Effective phosphors effectively retain their ions, minimizing energy loss through non-radiative transitions. The presence of contaminant ions can absorb or redirect energy, thereby impeding the material's luminescent properties.

Phosphor materials are evaluated based on several crucial factors, including the range of emitting colors (such as red, green, and blue), lumen equivalency, emission spectrum, quantum yield, and emission lifespan. Color points are determined by dividing the emission spectrum energy using the Commission Internationale de l'Eclairage (CIE) graphical rule. A higher luminosity count indicates a brighter light, and phosphors should have a higher lumen equivalence. The emission spectrum of electromagnetic radiation is generated when an atom or molecule undergoes a transition from a higher to a lower energy level. It is important for phosphors to have a long emission lifespan in order to be economically viable. Quantum efficiency measures the quantity and wavelengths of emitted photons from a phosphor in relation to the number of triggering photons at specific wavelengths. The decay time, also known as afterglow or persistence, refers to the time it takes for the emission intensity to decrease to 10% of its initial intensity after stimulation ceases. Rare earth ions such as Tb^{3+} , Eu^{2+} , Dy^{3+} , Mn^{2+} , and Eu^{3+} exemplify the utilization of d-electrons in phosphors. These ions interact favourably with the crystalline host lattice through their d-orbitals. Several crucial characteristics need to be assessed to determine the suitability of synthesized phosphors for further applications. Factors such as chemical and thermal stability, quantum efficiency, color point, biodegradability, emission spectrum, and longevity play significant roles in this evaluation. Phosphor materials find applications in various technologies including

plasma and field-emission displays, LEDs, solar cells, thermal sensors, and other diverse fields.

1.2 Host matrix and activator ions

Phosphors components are a host matrix and an activator, which serves as the radiating core. Inorganic hosts possess desirable properties such as physical, thermal, and chemical inertness, making them ideal candidates. However, self-activated hosts are preferred over inorganic hosts as they exhibit their own intense and broad visible radiation when stimulated by UV light. This inherent radiation is utilized by the activator to enhance the emission intensity.

The activator serves as a dopant, introduced into the crystal of the material to create the desired type of inhomogeneity. The presence of activators influences the emission delay time. The concentration of activators within the crystals is also a crucial factor to consider. While the host material is typically microcrystalline and transparent to visible light, the activators are responsible for absorbing and emitting radiation.

The activator plays a crucial role in collecting and amplifying the stimulating radiation, leading to an excited state. Not all ions or elements exhibit luminescence. These factors determine the ability of luminescent compounds to convert light. To achieve narrow-band luminescence in the visible spectrum, RE elements are commonly utilized. The performance criterion for these elements is light emission, which is possible due to their unique electronic structure that allows for efficient response to high-energy stimulation such as gamma rays and X-rays. RE phosphors are often effectively excited by deep UV wavelengths.

Recently, there has been increased interest in the illuminance of trivalent RE ions (Sm^{3+} , Dy^{3+} and Eu^{3+}) in silicates because of their good chemical and thermal stability, wide UV transparency, high luminous efficiency, and low composite temperature.

Various materials like oxides, nitrates, silicates, vanadates and molybdates are used as the host but silicates are preferred as they possess high chemical and physical stability. Silicates have high temperature strength, and chemical inertness which makes them strong candidates for many practical applications.

RE ions are doped in a variety of materials are employed as activator ions for phosphor. Dy^{3+} activated luminescent materials have attracted a lot of attention since they might be used as single-phase white light emitting phosphors. The selection of Dy^{3+} as a dopant is motivated by several factors:

1. Cost-effectiveness
2. Suitable Color Rendering Index (CRI)
3. Thermal and chemical stability

1.3 White light emitting diodes (w-LEDs)

A good amount of portion of the total energy generated across industries is used for both indoor and outdoor lighting. Typical incandescent and fluorescent lighting uses either gas discharge or heat. Due to the high temperatures involved, both phenomena are linked to significant energy loss. Along with energy efficiency, it's crucial to guarantee that the lighting technology is environmentally friendly. There is no prominent option than solid-state lighting if all of these requirements must be met. It is based on light-emitting diodes, which are essentially semiconductor chips with p-n junctions that are forward biased to emit light. Luminous efficacy, low power dissipation, persistence, environmental friendliness, and a lasting operative lifetime are just a few of the wonderful advantages that phosphor-converted light emitting diodes (pc-LEDs) have over other traditional sources of lighting. Most of the w-LEDs on the market today employ a blue-emitting (450–470 nm) diode to activate a $\text{Y}_3\text{Al}_5\text{O}_{12}:\text{Ce}^{3+}$ (YAG:Ce) phosphor, causing it to produce yellow light. However, the lack of the red component in this method results in low and high CRI and CCT values respectively, in the light that is produced. A common technique for producing white light is to coat an n-UV LED chip with RGB (red, green, and blue) phosphors. But it is not an easy task to maintain the proper ratio of red, blue and green colour emitting phosphors to obtain resultant white emission and use of three phosphors requires a greater number of dopants that increases the cost of LEDs[1].

1.4 Photoluminescence (PL)

Photoluminescence refers to the emission of light by a substance after it has been exposed to light. The term "photoluminescence" is derived from the Latin word "luminescence" and the Greek suffix "photo," meaning "light." PL occurs when a substance absorbs photons, resulting in the generation of light. This process involves the absorption of a visible-range photon by a particle, which excites an electron to a higher energy level, followed by the subsequent emission of a photon as the electron transitions to a lower-energy state.

The experimental technique of photoluminescence (PL) is employed to study and characterize semiconductor nanostructures, as well as investigate their electrical properties. Photoluminescence is induced when the energy of incident photons exceeds the bandgap energy of the material. To observe PL, the wavelength of the incident light should be close to the bandgap wavelength.

The PL spectrum, device temperature, and intensity, which is influenced by the irradiation intensity, provide essential data for device characterization. The photoluminescence spectrum of a semiconductor, such as GaAs, exhibits multiple distinct transitions. Therefore, the PL spectrum of GaAs becomes more complex as the material becomes purer.

To analyze the PL spectrum resulting from the formation of impurities and defects, a comprehensive understanding of the energy levels is essential. It is a valuable characterization technique due to the extensive amount of data it offers.

PL offers several advantages, such as rapid and easy generation of large amounts of data, indirect assessment of non-radiative recombination time, and the provision of information about energy levels and sensitivity of the system.

It is a non-destructive technique used for labeling, staining, chemical marking, and

revealing cosmic-ray tracks in crystals.

Fluorescent lights and LEDs are widely used examples, where fluorescent coatings convert short wavelength UV (blue) light into longer wavelength (yellow) light.

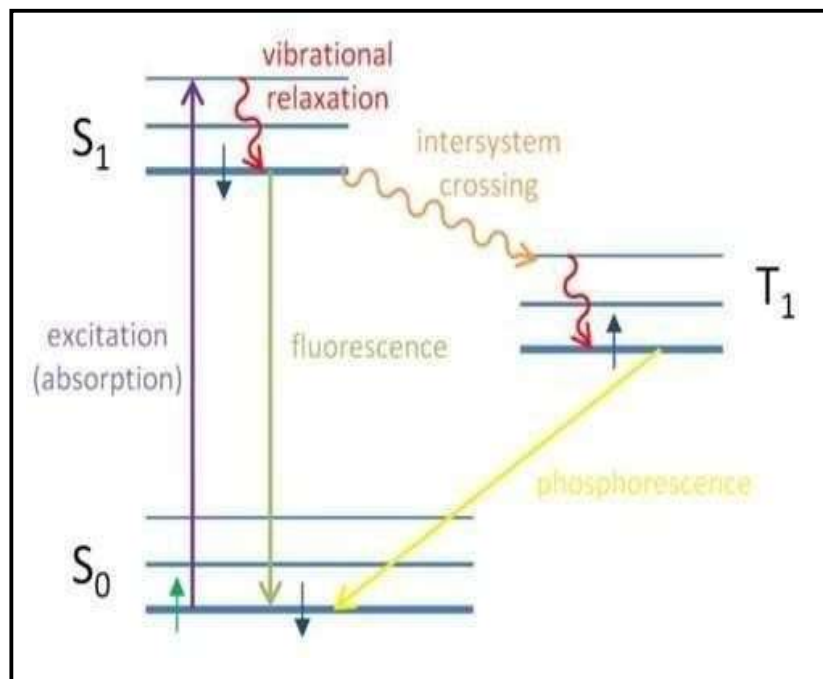


Fig. 1.2. Jablonski diagram of fluorescence and phosphorescence processes

The molecule can undergo intersystem crossover (ISC) to the excited triplet state (T_1). ISC occurs when molecules possess significant spin-orbit coupling, which is often observed in heavy metals like europium and iridium due to their strong spin-orbit coupling strength. In the absence of spin-orbit coupling, the decay from the T_1 state to the ground state (S_0) is a forbidden transition according to angular momentum conservation, as the states have different spin multiplicities. However, the presence of spin-orbit coupling overcomes this restriction, allowing the transition from T_1 to a higher-energy singlet state (S_1) to occur. The transition from T_1 to S_0 is typically "prohibited," resulting in a long decay time, a phenomenon known as phosphorescence, as depicted in Fig. 1.2.

1.5 Fluorescence and phosphorescence

Fluorescence refers to the rapid emission of light (photoluminescence) that occurs immediately after a material has been excited by photons. On the other hand, phosphorescence refers to long-lasting photoluminescence that continues even after the excitation source has been removed. In essence, fluorescence is a type of photoluminescence that does not require a change in spin multiplicity during the radiative transition, while phosphorescence requires change in spin multiplicity.

Molecules that possess paired electrons are generally stable, while those with unpaired electrons tend to be highly reactive and volatile. Electrons possess an intrinsic angular momentum known as spin, and the spin symmetry determines the possible states of an electron. When two spins are arranged in an anti-symmetric manner, the total spin is zero ($S = 0$), indicating a singlet state.

Conversely, when the spins are arranged symmetrically, the total spin is one ($S = 1$), representing a triplet state. Singlet refers to the anti-symmetric arrangement of electron spin pairs with a total spin of zero, while triplet refers to the three symmetric arrangements of spin pairs with a total spin of one. When a photon is absorbed, one of the electrons in the electron pair is excited to a higher energy level, causing the molecule to be in an elevated energy state. The molecule's ground energy level is referred to as the singlet state (S_0), and the photoexcited state must also be a singlet state due to the conservation of angular momentum (S_1). The decay from the S_1 state to the S_0 state is a permissible transition (as the spin multiplicities are identical), resulting in fluorescence occurring on a time scale ranging from picoseconds to nanoseconds.

Fluorescence finds practical applications in various fields such as mineralogy, gemology, drug research, sensors, and the production of 3D images displayed on a monitor by directing the fluorescence at electrons. In order to tightly secure samples in a specimen container, a conductive adhesive is commonly used.

CHAPTER 2: INSTRUMENTATION

2.1 X-ray diffraction (XRD)

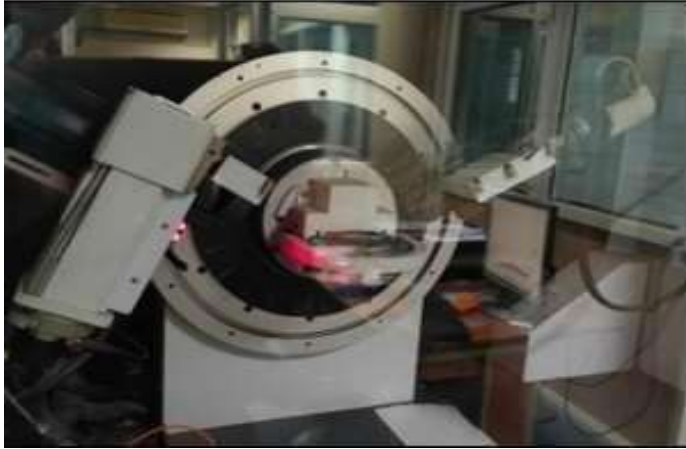


Fig. 2.1. X-ray diffraction

X-ray diffraction (XRD) is a widely used and important technique for the characterization of materials. As advancements in material science technology continue to occur and new materials are being developed, there is a need to update existing analytical methods to effectively address emerging complex challenges. This allows for the exploration and resolution of intricate issues that arise in the characterization of these new materials. Even though X-ray diffraction (XRD) is a well-respected non-destructive method, its characterisation skills still need to be improved, particularly when working with complicated mineral formations. This comprehensive review addresses various aspects of XRD analysis, including crystal structure determination, XRD standards, applications, potential vulnerabilities, and necessary safety precautions. The review also explores future research directions, particularly the utilization of artificial intelligence (AI) and

crystallite size, crystalline structure, size and orientation, interplanar spacing, phase identification, and shape, information about lattice parameters, residual stress and strain, and thermal expansion coefficient of materials. By compiling these important discussions on XRD analysis for mineral characterization, this review aims to assist professionals and researchers in the chemical, mining, iron, metallurgy, and steel industries. This scattering process involves the dynamic interaction between X-ray photons and the atomic structure of the material. A key principle in X-ray diffraction is Bragg's law, which describes the conditions for constructive interference of scattered monochromatic X-rays. According to Bragg's law, when the scattered X-rays are in phase, they produce constructive interference, leading to the formation of diffraction patterns as shown by equation (2.1) below.

$$n\lambda=2d\sin\theta \quad (2.1)$$

To identify an unknown substance using X-ray diffraction, a diffractometer is used to record the powder diffraction pattern. This pattern contains diffraction bands with corresponding d-values and related energies. These values are then compared to the line patterns available in Powder Diffraction File (PDF) databases, which contain information on various compounds. By matching the experimental data with the known patterns in the database, the unknown substance can be identified. The value of the crystal plane spacing, denoted as d, can be estimated using the given angles between the incident beam and the perpendicular to the reflective lattice plane. By measuring the angles of each crystallographic phase, along with the degree of reflection and the wavelength of the incident beam, the spacing between the crystal planes can be calculated.

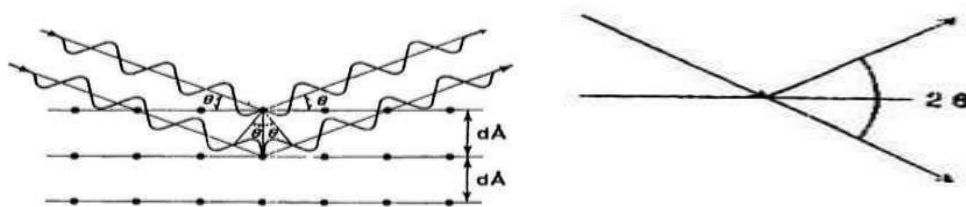


Fig. 2.2. Schematic representation of Bragg's law

To confirm the presence of a crystalline structure in a substance, whether it is a uniform material or an inhomogeneous mixture, the identification of characteristic diffraction lines is necessary. These diffraction lines correspond to specific lattice planes within the crystal structure and can be analyzed to determine the crystallographic phases present.

Production of Xray

X-rays are found in the region of the electromagnetic energy spectrum that lies between ultraviolet and gamma rays. The wavelength of X-rays ranges from 10.0 to 0.1 Angstrom. They are created when rapidly moving electrons with enough energy are slowed down. Electrons are drawn to a metal target (the anode) by the high voltage that is maintained across the electrodes of an x-ray tube. At the point of collision, X-rays are generated and released in every direction. Electromagnetic energy (x-rays) is produced by the conversion of electron kinetic energy.

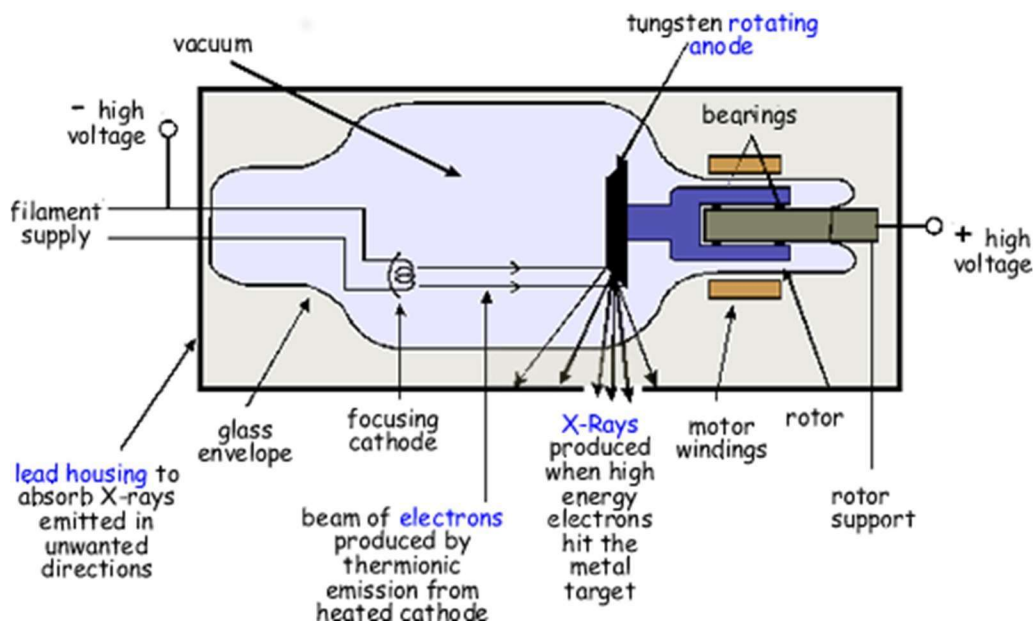


Fig.2.3. X ray tube

2.1.1 Joint committee on powder diffraction standards (JCPDS)

In 1941, the Joint Committee on Powder Diffraction Standards (JCPDS) was established to maintain the Powder Diffraction File (PDF). The PDF is a database that contains information on powder X-ray diffraction patterns, including the relative intensities of prominent diffraction peaks at specific d- spacings. It is widely utilized for material classification based on X-ray diffraction patterns and is designed for various applications. Currently, it is known as the International Centre for Diffraction Data (ICDD). The PDF, particularly the 2019 edition, consists of distinct sets of material data. Each data set includes diffraction patterns, sample requirements, research and literature data, as well as laboratory, instrumental, crystallographic, and relevant mechanical properties presented in a standardized format[2].

2.2 Scanning electron microscope (SEM)

It is a method for analyzing the morphologies of a material or sample. This is because it is necessary to first determine whether the data corresponds with the reference, peaks, and indexes. After it has been shown that the sample material has correctly crystallized, the previously mentioned scanning electron microscope is used. The signals that are created by the electrons' interactions with the atoms in the specimen contain details about its morphology, structure, and crystallography in addition to its surface topography and surface characteristics. The sample is inspected by the electron beam in scanning electron microscopy using a raster technique. The electrons at the top of the column originate from the electron source[3,4].



Fig.2.4. Scanning electron microscope (SEM)

They are released when the thermal energy exceeds the work function of the reference element. The anode causes them to become stimulated and activated (positively charged). To shield the electron column from vibrations, noise, and pollutants, the entire column must be encased in a vacuum. The detector can collect more electrons in the vacuum while maintaining a clear picture for the user. The electrons' direction can be changed via lenses. Two electromagnetic lenses are used in it. The beam is collected by the condenser lens and then changed by the objective lens before striking the sample

2.3 Fourier infrared transform spectroscopy (FT-IR) Analysis

Using a Fourier Transform Infrared (FT-IR) instrument, infrared light is steered through a substance in this manner. A portion of the light is absorbed by the sample as it travels through the material, while the remaining portion goes through. A spectrum that depicts how the infrared light interacts with the sample is the output that is produced at the detector. This spectrum gives important details about the chemical makeup of the substance and usually spans wavenumbers from 4000 cm^{-1} to 400 cm^{-1} . Every molecule possesses a distinct spectral fingerprint, which is an infrared absorption band pattern. Now, one could think that recording a spectrum in terms of energy vs time is strange, unless one considers the correlation between time and frequency: they are reciprocal.

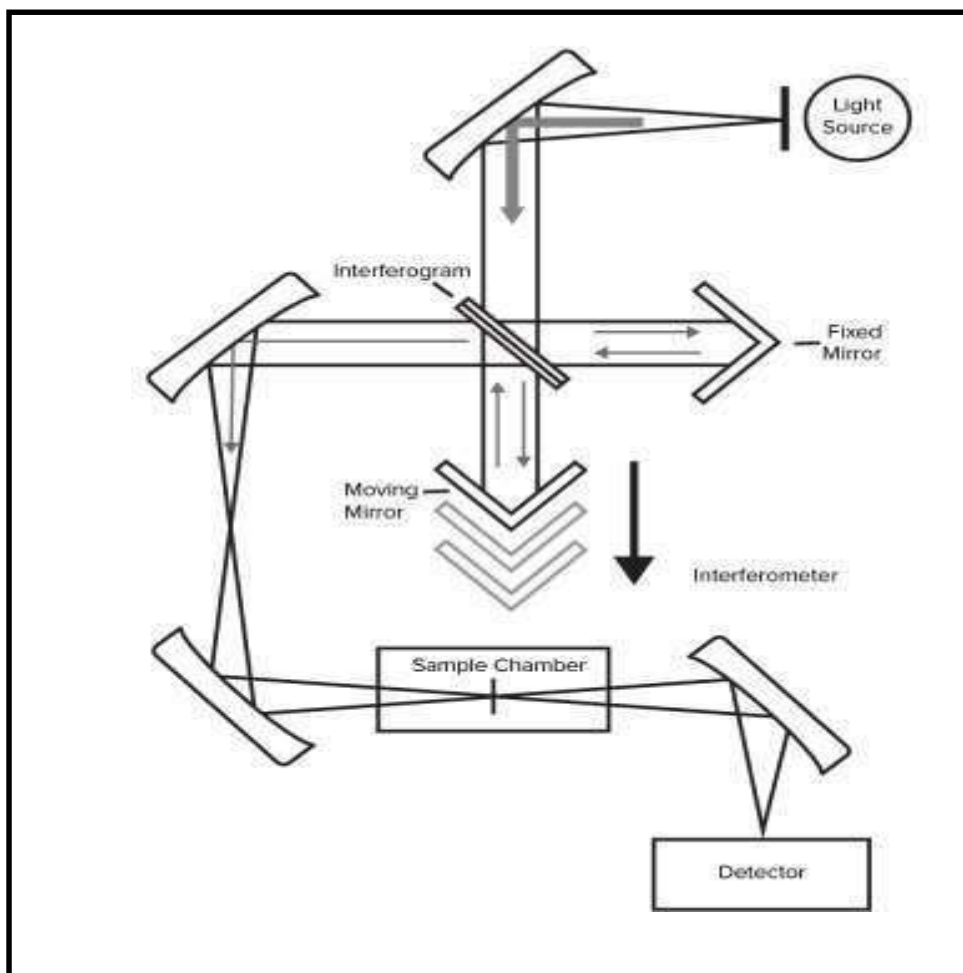


Fig.2.5. Parts of an FTIR spectrometer with source, interferometer & detector.

Using the Fourier transform (FT) function, an I-vs-t spectrum can be transformed to an I-vs- ν spectrum. The FT can be given by the expression:

$$A(r) = \sum X(k) \exp \left(-2\pi \frac{irk}{N} \right) \quad (2.2)$$

here, $A(r)$ are the frequency domain & $X(k)$ are the time domain points and N are the total points in the spectrum. Because each functional group has its own distinct vibrational energy that may be utilized to identify a molecule by combining all of the functional groups, FTIR microscopy is an excellent tool for identifying samples, characterization of multilayer films, and particle analysis. Because each functional group is made up of distinct atoms with variable bond strengths, each of these functional groups, and categories of functional groups, has its own set of vibrations. Because each molecule's collection of

vibrational energy bands is distinct, these peaks can be utilized to identify the functional groups involved utilizing literature analyses of large sample datasets.

2.4 Diffuse reflectance spectroscopy (DRS)

The diffuse reflectance spectroscopy is the most common technique for examining the spectrum characteristics of opaque solid materials is spectroscopy. Its foundation is the idea that when light strikes a substance, some of it experiences specular reflection and interacts with the material's bulk, while the remaining portion of the light is reflected inward surface reflection.



Fig. 2.6. Diffuse Reflectance Spectroscopy

2.5 Photoluminescence spectrometer

In photoluminescence spectrometer, light is directed onto a specimen; here it is absorbed and photosensitization may take place, resulting in the emission of photoluminescence. The chromatic aberration spot width of a concentrated laser beam is of the order of 1 m for spatially resolved micro-PL at room and the lowest temperature. When scanning the sample, a CCD camera records the spectrum for each location that was looked at. Examine the emission, quantum yield, luminescence energy transfer, diffuse duration, chemical/physical durability, and other parameters while using luminous materials.



Fig.2.7. Photoluminescence spectrometer

CHAPTER 3: EXPERIMENTAL PROCEDURE

3.1 Phosphor Preparation: Materials and Method

The KMM: $x\text{Dy}^{3+}$ ($1 \leq x \leq 5$, $\Delta x = 1$), represented by KMM Dy 1.00, KMM Dy 2.00, KMM Dy 3.00, KMM Dy 4.00 and KMM Dy 5.00 respectively) were prepared using traditional solid state synthesis route. The starting materials were potassium carbonate (K_2CO_3 , 99.9%), magnesium oxide (MgO 99.9%), Molybdenum trioxide (MoO_3 , 99.99%) and dysprosium oxide (Dy_2O_3 99.9%). The raw materials were thoroughly combined and pounded for an hour using an agate mortar and pestle after initially being weighed in line with the nominal content of phosphor. The ground samples were kept in alumina crucibles and then heated at 750°C for 8 hrs in an electric furnace. After cooling down, the final products were ground once again for further characterizations.

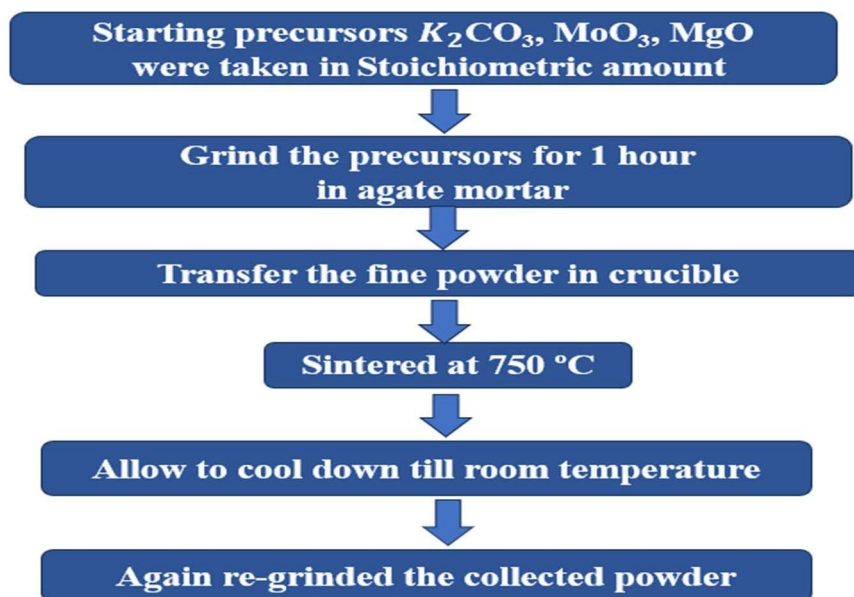


Fig.3.1. Flow chart of synthesis procedure of KMM: $x\text{Dy}^{3+}$ ($1.0 \leq x \leq 5.0$ mol%, $\Delta x = 1.0$ mol%).

CHAPTER 4: RESULTS AND DISCUSSION

4.1 Structural and elemental studies

4.1.1 XRD Analysis

Fig 4.1. depicts the XRD pattern of undoped KMM phosphors. The XRD patterns show complete agreement with standard data received from the Joint Committee on Powder Diffraction Standards (JCPDS-84-0155)[5,6].

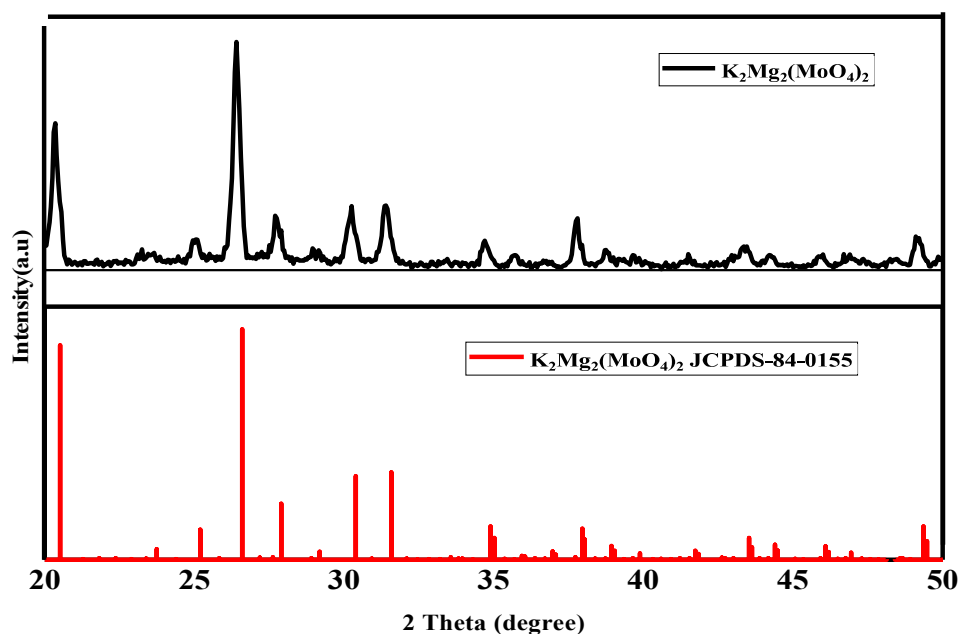


Figure 4.1: XRD pattern of undoped phosphor compared with typical JCPDS data

4.1.2 Morphology features

The shape and particle size of KMM phosphor are examined using FE-SEM technique, with agglomeration observed in undoped and 4.0mol% Dy^{3+} doped KMM phosphor.

Particle size ranges from 2-6 μm , calculated using ImageJ software. Particle agglomeration is caused by high-temperature reaction and manual grinding. Energy-dispersive X-ray spectroscopy (EDX) is used to examine the elemental makeup and purity of annealed samples, revealing all precursor elements present in the phosphor lattice[7].

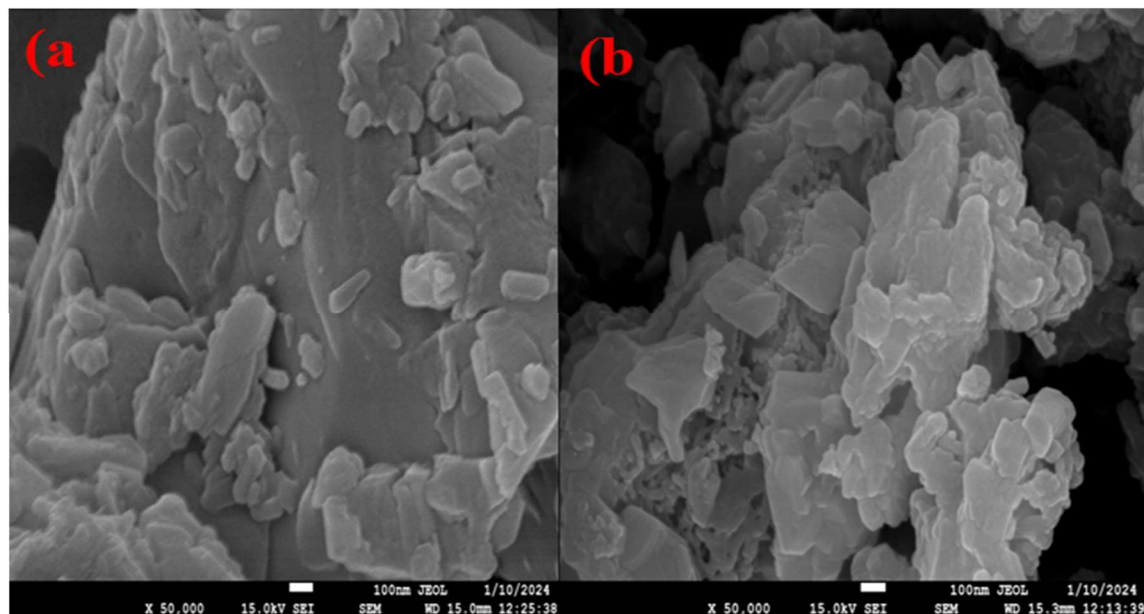


Fig.4.1(a): SEM images recorded for $\text{K}_2\text{Mg}_2(\text{MoO}_4)_3: x \text{Dy}^{3+}$ ($x=0, 4 \text{ mol } \%$) phosphor.

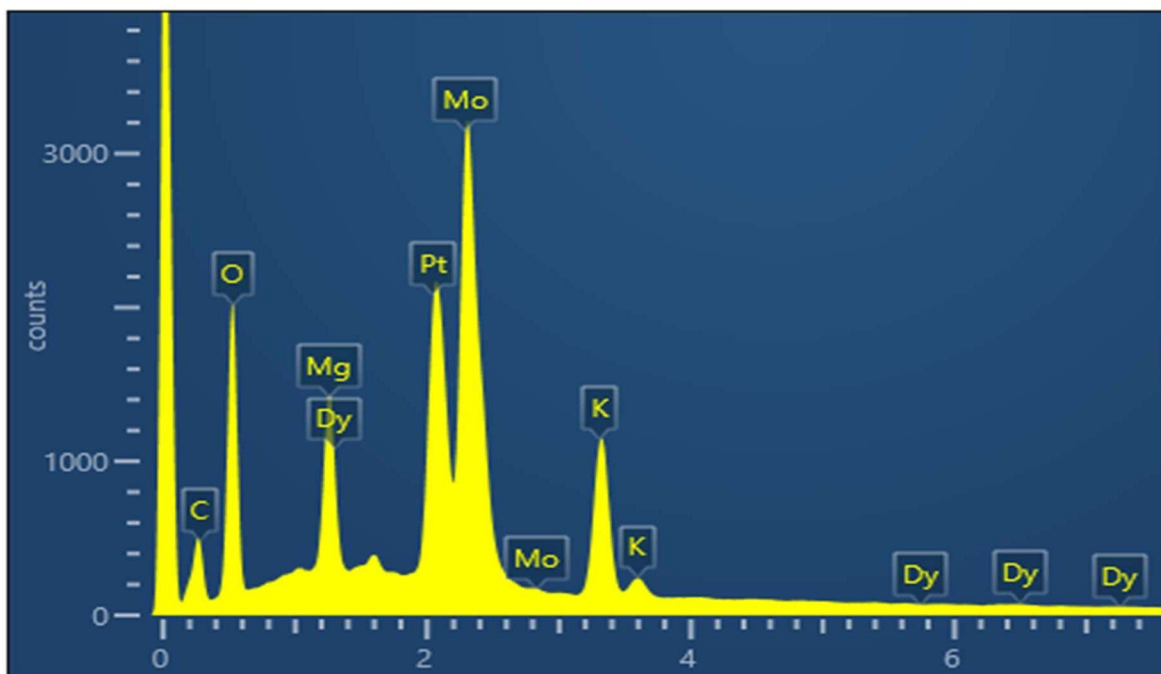


Fig.4.2: EDX image of the $K_2Mg_2(MoO_4)_3 \cdot x Dy^{3+}$ ($x= 4$ mol %) phosphor.

4.1.3 FTIR Analysis

The FTIR spectrum, which is displayed in above figure was acquired in the $400\text{--}4000\text{ cm}^{-1}$ area to identify the kind of bonding in KMM phosphor. The Mo-O asymmetric stretching mode vibration in MoO_4^{2-} tetrahedra was responsible for the intense bands seen at $725, 819, 880,$ and 937 cm^{-1} . The O-H stretching and H-OH bending vibrations are responsible for the bands at 1634 and 3752 cm^{-1} , respectively. The presence of hydroxyl groups is responsible for the bands seen at 2893 and 2979 cm^{-1} . So, using FTIR spectroscopy, the bonding found in KMM phosphor was confirmed[7,8].

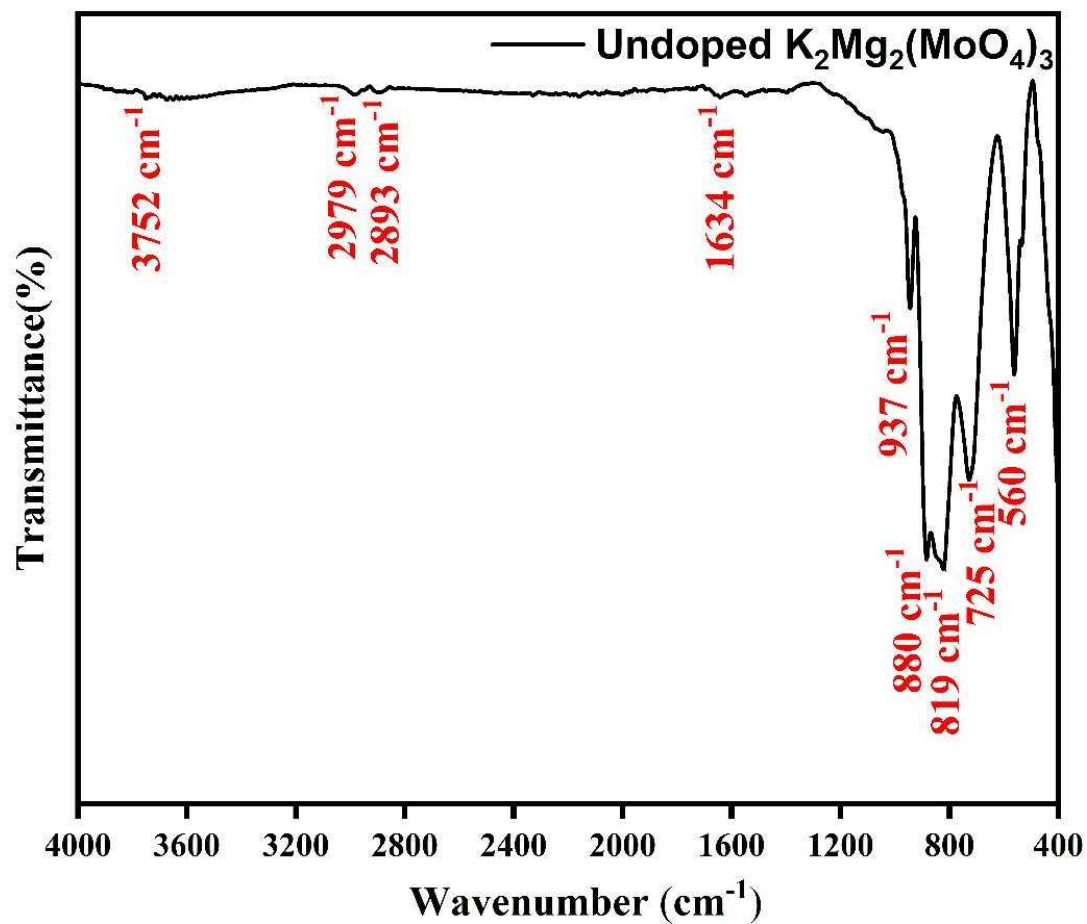


Fig.4.3: FTIR spectrum of an un-doped $K_2Mg_2(MoO_4)_3$ phosphor.

4.1.4 DRS and calculations for optical bandgap

Because it controls the energy of photons released when electrons recombine with holes in a semiconductor material, the optical bandgap is essential to LED technology.

Figure 4 displays the diffuse reflection spectrum (DRS) for the phosphors $KMM:xDy^{3+}$ ($1.0 \leq x \leq 5.0$, $\Delta x = 1.0$ mol %), which was obtained in the 200–1400 nm region.

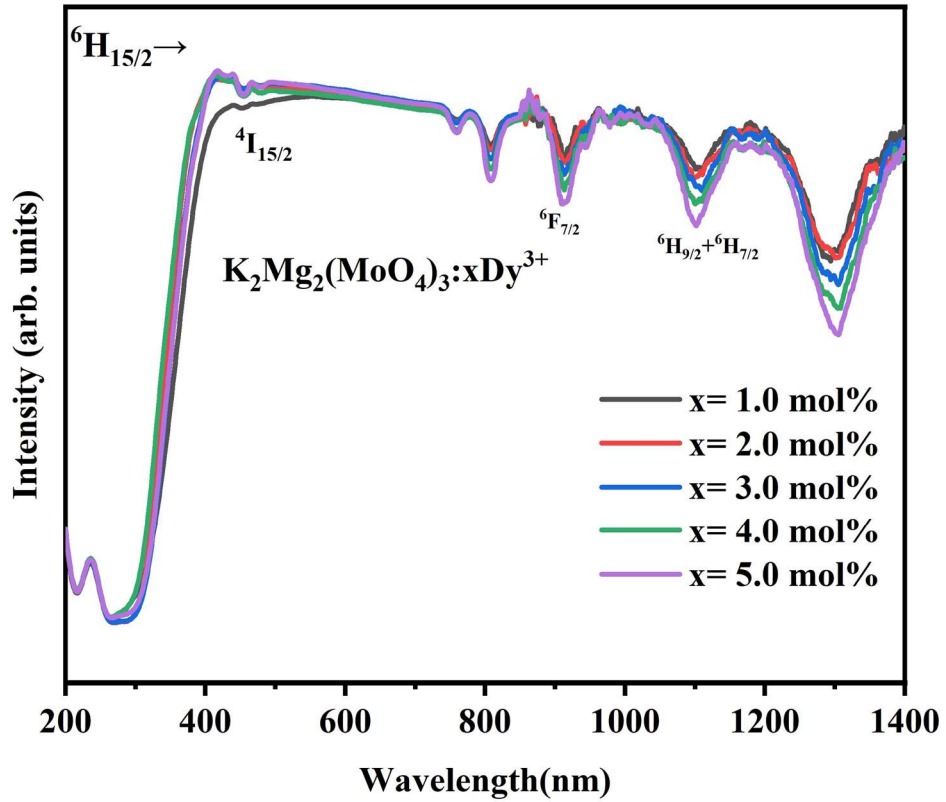


Fig.4.4: Diffuse reflectance spectra of $K_2Mg_2(MoO_4)_3 \cdot x Dy^{3+}$ ($1.0 \leq x \leq 5.0$, $\Delta x = 1.0$ mol %), phosphors.

The Kubelka-Munk equation below can be used to determine a material's bandgap from Diffuse Reflectance Spectroscopy (DRS) data.

$$F(R) = \frac{(1-R^2)}{2R} = \frac{\alpha}{S} \quad (4.1)$$

The Kubelka-Munk function is denoted by $F(R)$, reflectance by R , absorption coefficient by α , and dispersion coefficient by S . The bandgap energy (E_g) and absorption coefficient (α) are connected by the Tauc equation that can be expressed as follows.

$$\alpha h\nu = C(h\nu - E_g)^n \quad (4.2)$$

Photon energy is represented by $h\nu$, and the energy-independent constant by C . Because $F(R)$ is proportional to α , the formula above can be expressed as follows:

$$F(R)h\nu = C(h\nu - E_g)^n \quad (4.3)$$

Plotting the Tauc graph of $[F(R)]^{1/2}$ and $h\nu$ allowed us to determine KMM:Dy³⁺ band gap. When linear data is calculated into a straight line, the optical bandgap (E_g) is

obtained. As seen in Fig.4.5, the E_g values of KMM:xDy³⁺ ($1.0 \leq x \leq 5.0$, $\Delta x = 1.0$ mol %) phosphors are 5.55, 5.52, 5.51, 5.50, and 5.45 eV, in that order. This bandgap energy decline is due to the doping concentration of Dy³⁺ ions. The unit cell somewhat expands as a result of the dopant's presence in the host, widening the band gap and tending to shrink the conduction and valence bands. Higher energy levels are thereby activated in a greater number of atoms, and when these atoms revert to lower energy states, their emissions are greater.

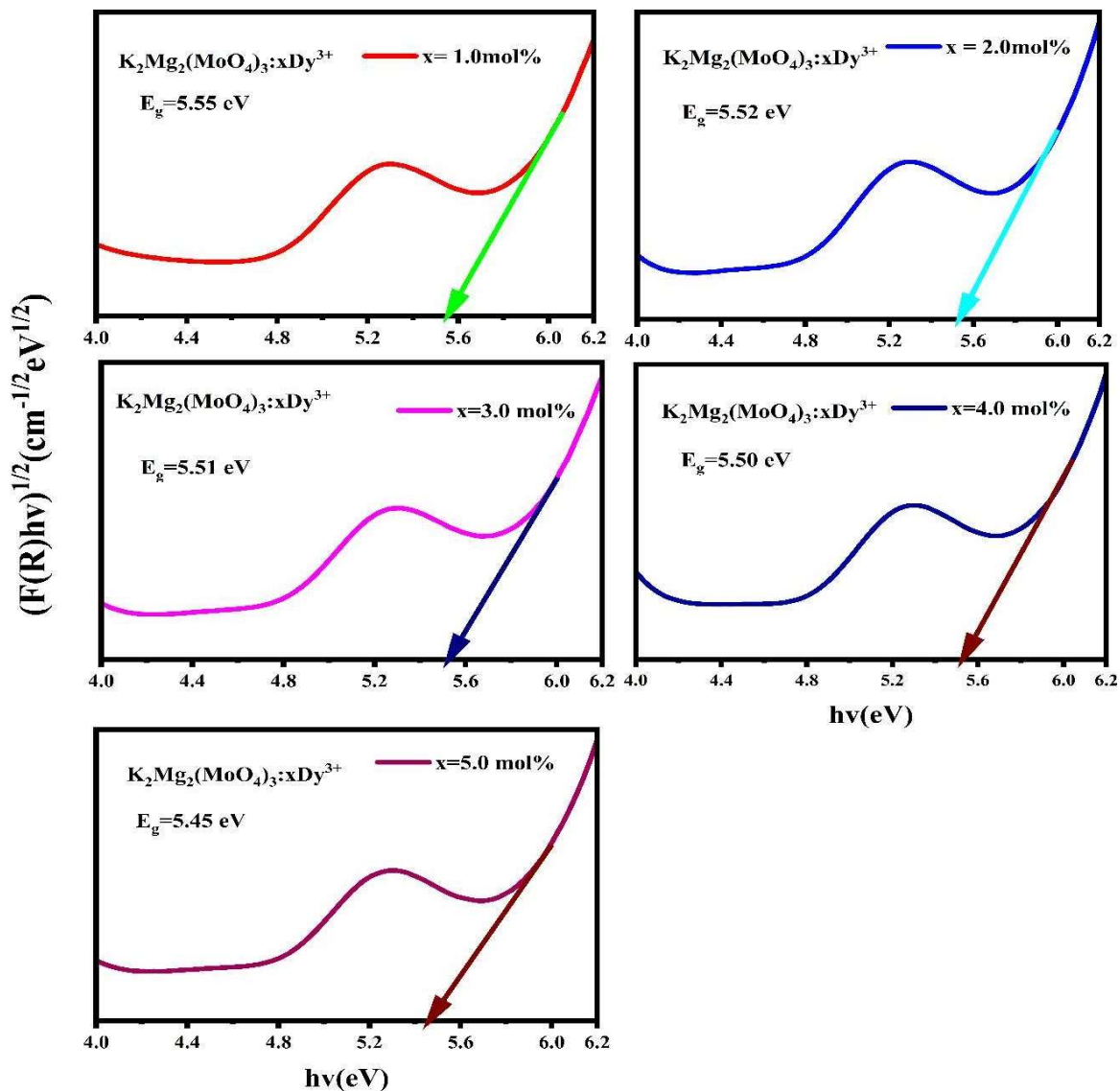


Fig.4.5: Tauc plots for direct optical band gap calculation.

4.1.2 Photoluminescence

For analysing, the photoluminescence spectrum of KMM, it is important to determine the excitation wavelength. The excitation spectra of as prepared KMM: Dy^{3+} ions doped phosphor in the 300-500 nm range observed at 576 nm emission wavelength is shown in Fig.4.6. The spectra consist of 12 peaks at 325, 338, 352, 366, 378, 387, 396, 425, 449, 452,

468 and 476 nm corresponding to a transition from ${}^6\text{H}_{15/2}$ ground state to ${}^6\text{P}_{3/2}$, ${}^6\text{P}_{5/2}$, ${}^6\text{P}_{5/2}$, ${}^4\text{I}_{13/2}$, ${}^4\text{I}_{11/2}$, ${}^4\text{M}_{21/2}$, ${}^4\text{G}_{11/2}$, ${}^4\text{I}_{15/2}$, ${}^4\text{I}_{15/2}$, ${}^4\text{F}_{9/2}$ and ${}^4\text{F}_{9/2}$ excited states respectively showing that a near UV wavelength can be used to excite Dy^{3+} ions. Among all observed peaks, the highest peak corresponds to 387 nm and is ascribed to the transition ${}^4\text{H}_{15/2} \rightarrow {}^4\text{I}_{15/2}$. Therefore, this wavelength was used for analysing the PL emission spectra of all the prepared $\text{K}_2\text{Mg}_2(\text{MoO}_4)_3:\text{Dy}^{3+}$ samples.

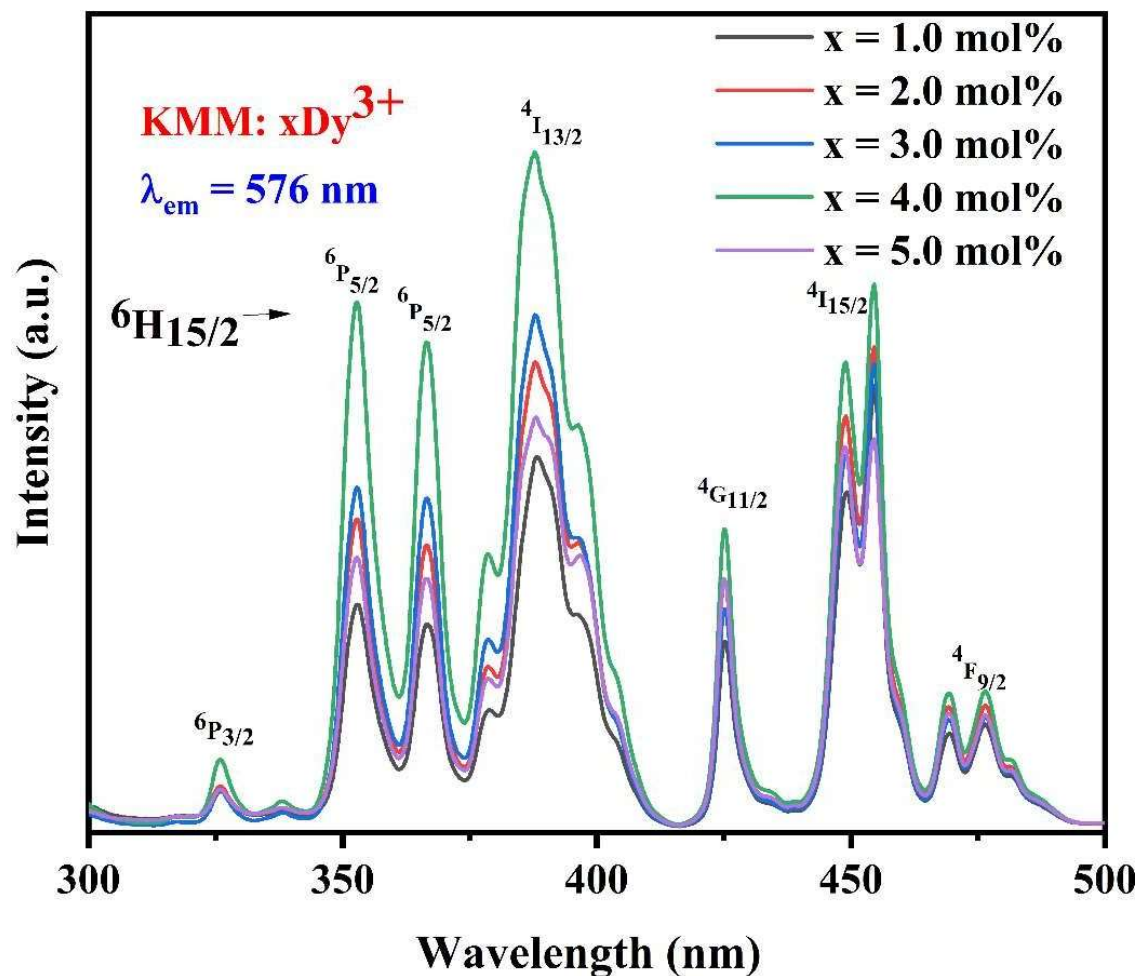


Fig.4.6: PL excitation spectra of Dy^{3+} ions doped $\text{K}_2\text{Mg}_2(\text{MoO}_4)_3$ phosphors under 576 nm emission wavelength.

The emission spectra of: $\text{KMM}:\text{Dy}^{3+}$ samples were recorded at 387 nm (excitation wavelength) and have been presented in Fig.4.7. There are 5 peaks at 475, 481, 486, 576 and

669 nm corresponding to the transitions from ${}^4F_{9/2}$ ground state to ${}^6H_{15/2}$, ${}^6H_{13/2}$, ${}^6H_{11/2}$ excited states respectively[9–11]. The shielding effect on 4f electrons on Dy^{3+} ions due to 5s and 5p outer electrons increases the stability of the electric field in the material, and the change in Dy^{3+} ion concentration has no significant effect on the position and shape of the bands in the spectra. The yellow band present at 576 nm (${}^4F_{9/2} \rightarrow {}^6H_{13/2}$) is the most intense among all the transitions. The spectral intensities of the bands in the PL spectra corresponding to these transitions increased with Dy^{3+} ions concentrations up to 4 mol% and then it subsequently decreases.

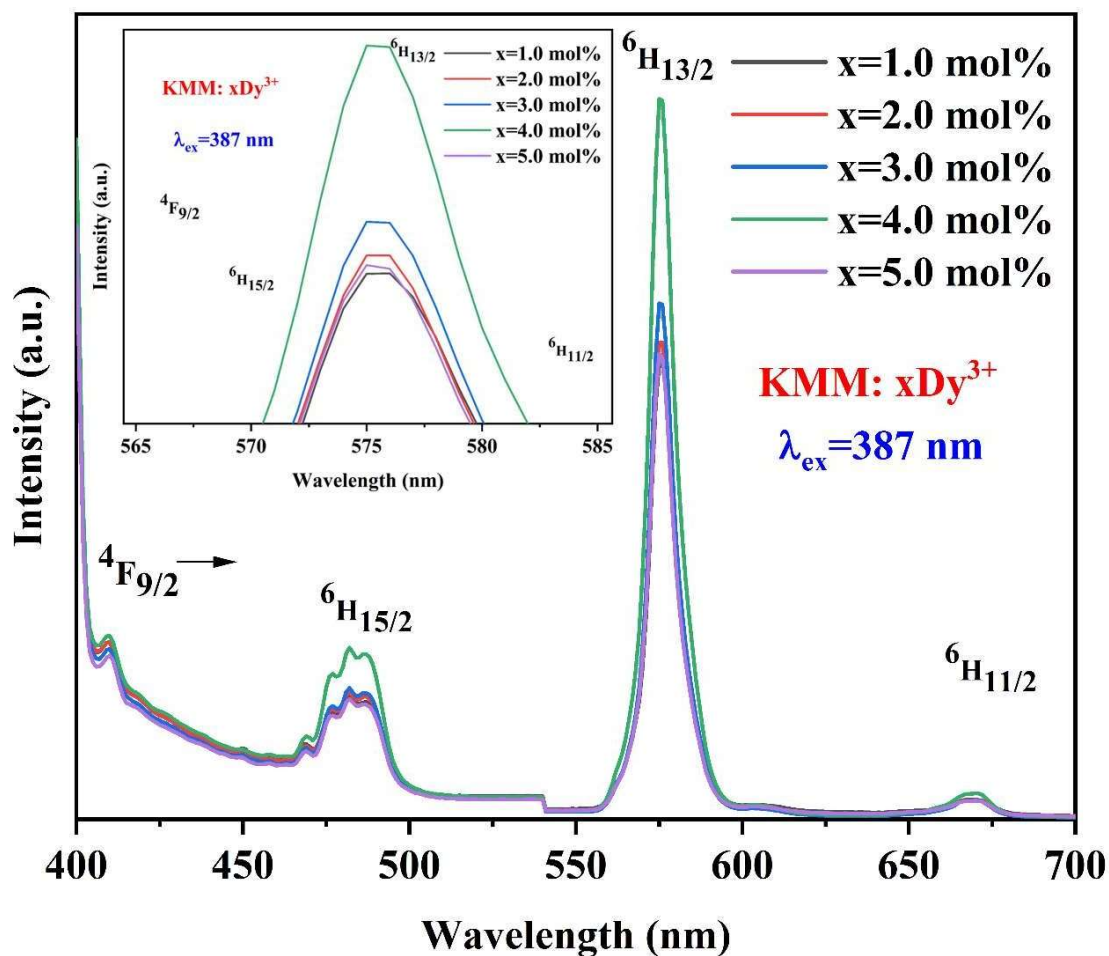


Fig.4.7 PL emission spectra of Dy^{3+} ions doped $K_2Mg_2(MoO_4)_3$ phosphors under 387 nm excitation wavelength.

Concentration quenching is the process responsible for the drop in PL band intensity observed when the Dy³⁺ ion concentration above 4.0 mol%. Concentration quenching is the process by which a material's luminescence diminishes as the concentration of activator ions rises above a certain point. Dy³⁺ ions are the activator in this instance. The mechanism of non-radiative energy transfer between luminescent/activator ions is typically the cause of concentration quenching. Due to electronic changes in their energy levels, Dy³⁺ ions frequently exhibit luminescence or light emission. On the other hand, non-radiative transfer may result via ion contact when Dy³⁺ ion concentration rises too high. Ion energy loss that occurs without the release of photons are referred to as non-radiative energy transfer [12,13].

As the concentration of Dy³⁺ rises, the distance between the two closest Dy³⁺ ions rapidly reduce, improving the contact between the surrounding Dy³⁺ ions and producing non-radiative energy transfer. The activator ions' exchange contact, multipole-multipole interaction, and radiation re-absorption all aid in concentration quenching. Using the Blasse equation: Dy³⁺ phosphors, we may ascertain the essential energy transfer between donor and acceptor ions in KMM [2,14–18].

$$R = 2 \left(\frac{3V}{4\pi K_c N} \right)^{1/3} \quad (4.4)$$

Here, V (3569.23 Å³) is the unit cell's volume, N is the number of ions (12) in the unit cell, and X_c is the mole% of Dy³⁺ ions (0.04) where quenching occurs. Between Dy³⁺ ions, the critical distance is estimated to be approximately 24.156 Å. Energy transfer via multipolar contact of Dy³⁺ ions will take place if the R_c value is higher than 5 Å. In essence, the interaction of RE ions in the solid matrix, where energy transfer takes place by electron exchange between ions is the subject of Dexter's theory of energy transfer. The type of multipolar interaction has been determined using the Dexter theory, which postulates a relationship between PL intensity and dopant concentration.

$$\log \frac{I}{x} = c - \frac{s \log(x)}{3} \quad (4.5)$$

where s is the index of electric interaction, which is 6, 8, and 10 for electric dipole-dipole, electric dipole-quadrupole, and electric quadrupole-quadrupole interaction, respectively, and

c is the constant for a host crystal, x is the dopant ion concentration, and I is the fluorescence

emission intensity. Figure 4.9 displays a plot of the intensity of Dy^{3+} emission as a function of $\log(I/x)$ vs $\log(x)$. This equation yielded a slope of 1.45 based on a linear fitting of the graph. As a result, the value of s is nearly 6, at 4.5. Consequently, it was determined that the primary mechanism for energy transfer between Dy^{3+} ions in KMM phosphor is the dipole-dipole interaction.

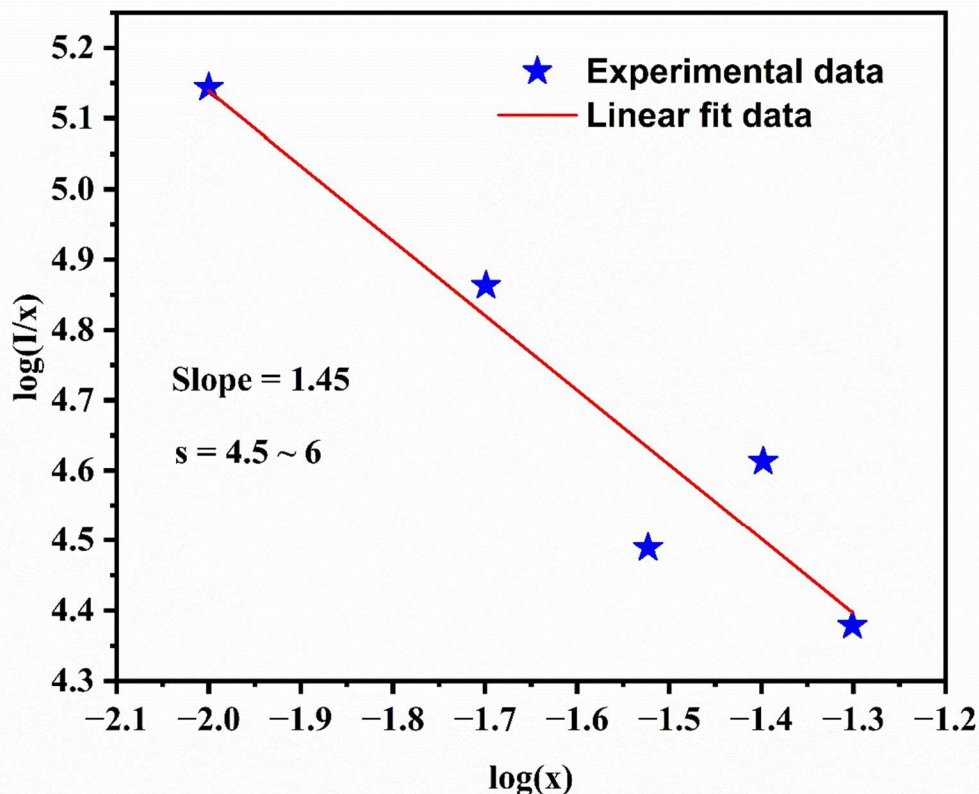


Fig.4.8. Dexter plot between $\log(1/x)$ and $\log(x)$

The phosphor's energy level diagram, which includes the emission, excitation, and energy transfer processes, is shown in Fig. 4.9. After being excited to a high energy level, Dy^{3+} ions instantly undergo non-radiative decay to return to the ${}^4\text{F}_{9/2}$ metastable state. As the electron enters the ${}^4\text{F}_{9/2}$ metastable state, the non-radiative transition releases some energy quickly. The degradation mechanism then causes Dy^{3+} ions to revert from ${}^4\text{F}_{9/2}$ to the lower states ${}^6\text{H}_{7/2}$, ${}^6\text{F}_{3/2}$, ${}^6\text{H}_{9/2}$, and ${}^6\text{F}_{1/2}$. The process of self-quenching and cross-relaxation channels

mechanisms (CRC) is explained by the decrease in the resonance energy transfer (RET) of Dy^{3+} ions[11].

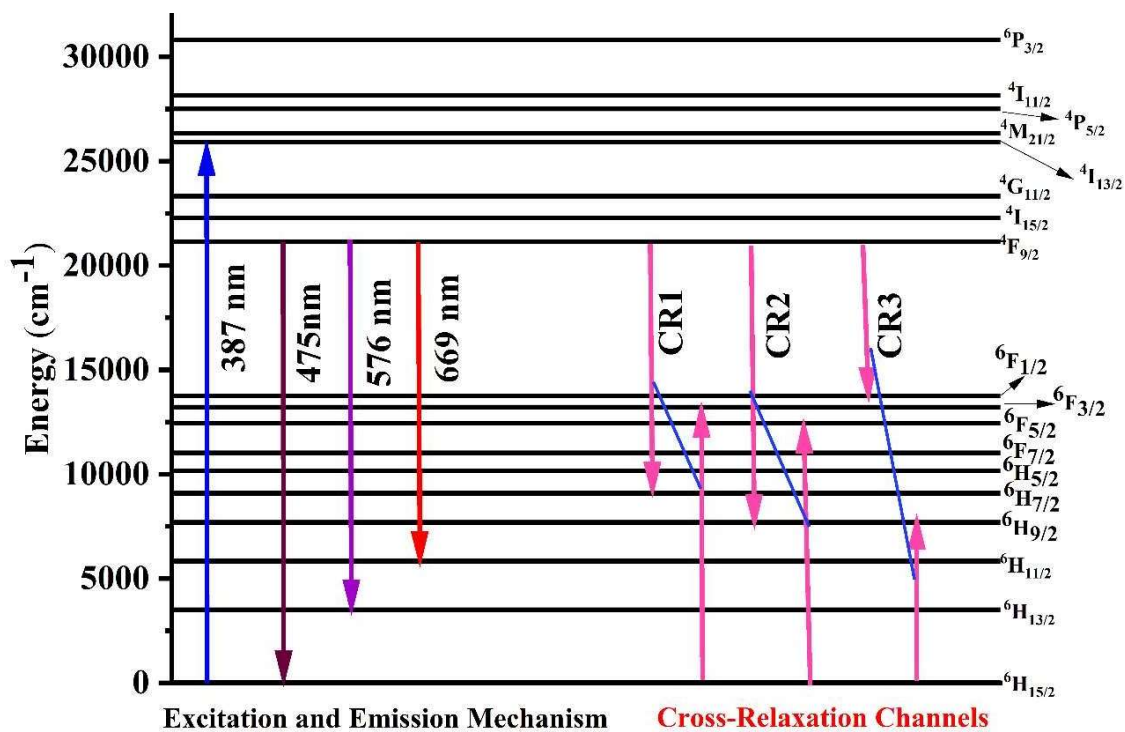
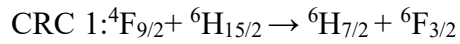


Fig.4.9. Partial energy level diagram and possible cross- relaxation channels of Dy^{3+} ion doped $K_2Mg_2(MoO_4)_3$ phosphor.

4.1.3 Y/B intensity ratio

The ratio of the yellow (Y) component's intensity to the blue (B) component's intensity is expressed by the Y/B intensity ratio. This ratio can reveal details about the characteristics of

the sample or its color composition when it is utilized in colorimetric analysis or imaging. By dividing the intensity of the yellow component by the intensity of the blue component, one can get this ratio. In a scientific setting, the Y/B ratio can be used to characterize and assess certain colors. It can be employed as a metric to evaluate the effects of studies, monitor changes over time, and differentiate between several samples. In a colorimetric examination, the Y/B intensity ratio provides a numerical representation of the proportion of blue to yellow component balance. Since the created KMM phosphor's Y/B intensity ratio is larger than 1, light is produced in the white area. The strong Y/B ratio validates Dy³⁺'s highly covalent nature. The electric dipole contribution will be large if the dominant interaction is the Stark effect brought on by an electric field.

In this instance, variations in the relative intensities of spectral lines will result from the electric dipole interaction's primary influence on the Yb intensity ratio. The magnetic dipole contribution will be large if the Zeeman effect brought on by a magnetic field is the dominating interaction. In the above case, the magnetic dipole interaction will be main factor influencing the Yb intensity ratio, leading to variations in the relative intensities of spectral lines. Therefore, KMM phosphor represents the largest Y/B value and therefore the highest covalent bond.

4.1.4 CIE coordinate analysis

An illustration of the precise way the human eye perceives light within a spectrum is called a chromaticity diagram. The luminosity coordinates of luminescent materials used in lighting applications are determined by the Commission Internationale de l'Eclairage (CIE). In this color space, each light's color may generally be expressed in (x, y) coordinates. Fig. 4.10. displays the CIE 1931 chromaticity coordinates of the phosphors listed. All of the samples have comparable color coordinates, as Table demonstrated. Correlated color temperature is another essential measure for proving the suitability and importance of RE³⁺ doped phosphor (CCT). The CCT represents the color hue of the light source when a phosphor is triggered by an energy source[5,19]. McCamy offered a method for calculating CCT as given below.

$$\text{CCT} = -449n^3 + 3525n^2 - 6823.2n + 5520.3$$

Here, $n = \frac{x-x_e}{y-y_e}$ and $x_e = 0.332$, $y_e = 0.186$. The CCT values determined from the PL spectra

recorded under 387 nm excitation wavelength corresponding to ($1.0 \leq x \leq 5.0$, $\Delta x = 1.0$ mol %) of Dy^{3+} ion concentration is tabulated in Table 4.2. All the results indicates that $\text{K}_2\text{Mg}_2(\text{MoO}_4)_3: \text{Dy}^{3+}$ phosphor is a promising white phosphor for w-LED applications. Color purity (CP) is another essential element in colorimetric calculations used to examine color saturation. The following formula can be used to estimate the CP[19,20].

$$CP = \frac{\sqrt{(x-x_{ee})^2 + (y-y_{ee})^2}}{[(x_d-x_{ee})^2 + (y_d-y_{ee})^2]} \quad (4.10)$$

where, (x_{ee}, y_{ee}) denotes equal energy point (x, y) is color coordinates of the $\text{K}_2\text{Mg}_2(\text{MoO}_4)_3$ phosphor and (x_d, y_d) denotes points of dominant wavelength. Under 387 nm excitation, it is observed that Dy^{3+} ($x = 4.0$ mol%) ions doped $\text{K}_2\text{Mg}_2(\text{MoO}_4)_3$ phosphor has 12% color purity. White light usually has a low color purity, while monochromatic sources usually have a high color purity.

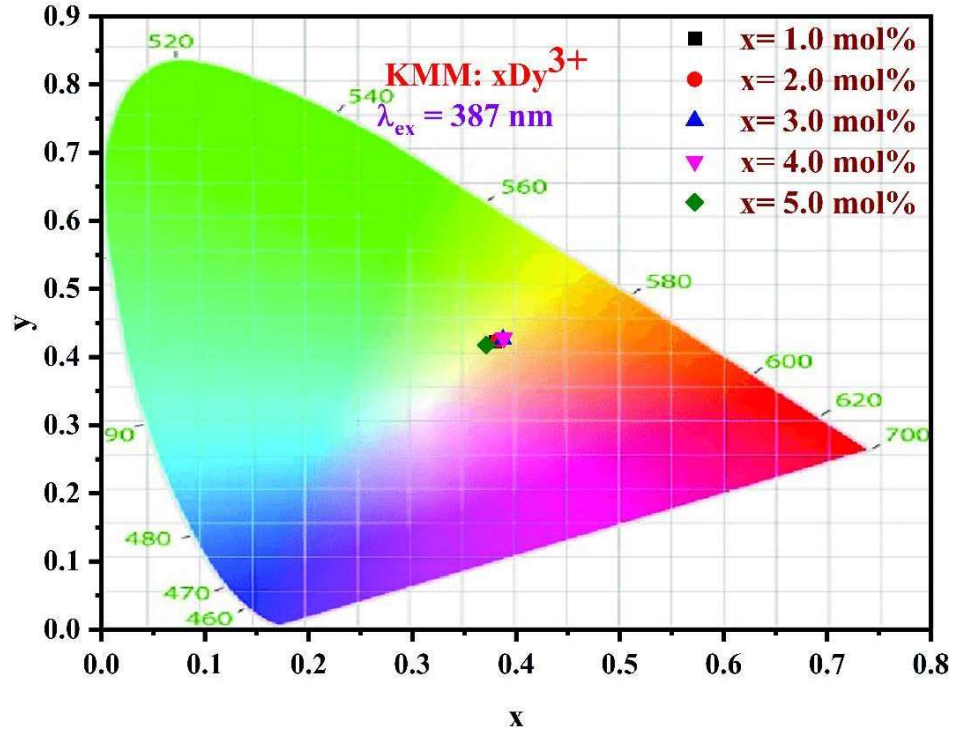


Fig.4.10. CIE chromaticity coordinates of Dy³⁺ ions in K₂Mg₂(MoO₄)₃ phosphors

Table 4.1

CIE coordinates, CCT values of KMM: xDy³⁺ (1.0 ≤ x ≤ 5.0, Δx = 1.0 mol %) under 387 nm excitation wavelength.

Sample ID	CIE coordinates	CCT values
KMM: xDy ³⁺	(x, y)	(K)
x = 1.0mol%	(0.380, 0.422)	4274.58
x = 2.0mol%	(0.383, 0.425)	4225.25
x = 3.0mol%	(0.387, 0.426)	4130.11
x = 4.0mol%	(0.388, 0.428)	4120.63
x = 5.0mol%	(0.371, 0.418)	4460.93

4.1.5 PL Decay Profile Analysis

The profiles of KMM's PL decay are shown in Fig.4.11. $x\text{Dy}^{3+}$ ($1.0 \leq x \leq 5.0$, $\Delta x = 1.0$ mol%) at room temperature with stimulation below 387 nm. The bi-exponential equation, which is defined below, demonstrated the best match for all concentrations of Dy^{3+} . This indicates that the host lattice's RE ions will most likely occupy two distinct crystallographic locations, and energy transfer from excited Dy^{3+} ions to unexcited Dy^{3+} ions are significantly interacting[4,6,21–23].

$$I = I_0 + A_1 * \exp\left(-\frac{t}{\tau_1}\right) + A_2 * \exp\left(-\frac{t}{\tau_2}\right) \quad (4.11)$$

where I stands for intensity of PL emission at t and I_0 stands for intensity of PL emission at $t=0$, where A_1 and A_2 stands for constant, τ_1 , τ_2 are luminescence decay lifetimes. The following equation might be used to calculate the average lifetime:

$$\tau_{\text{exp}} = \frac{A_1\tau_1^2 + A_2\tau_2^2}{A_1\tau_1 + A_2\tau_2} \quad (4.12)$$

The τ_{exp} values of $\text{K}_2\text{Mg}_2(\text{MoO}_4)_3: x\text{Dy}^{3+}$ ($1.0 \leq x \leq 5.0$, $\Delta x = 1.0$ mol %) were tabulated in Table 4.2. It was noticed that when the concentration of Dy^{3+} ions increased, as the values of τ_{exp} decreased. Energy exchange between Dy^{3+} - Dy^{3+} ions themselves at a closer distance may be the cause of decrease in lifetime values. The decay lifetimes obtained for all the given titles phosphors in the microsecond range.

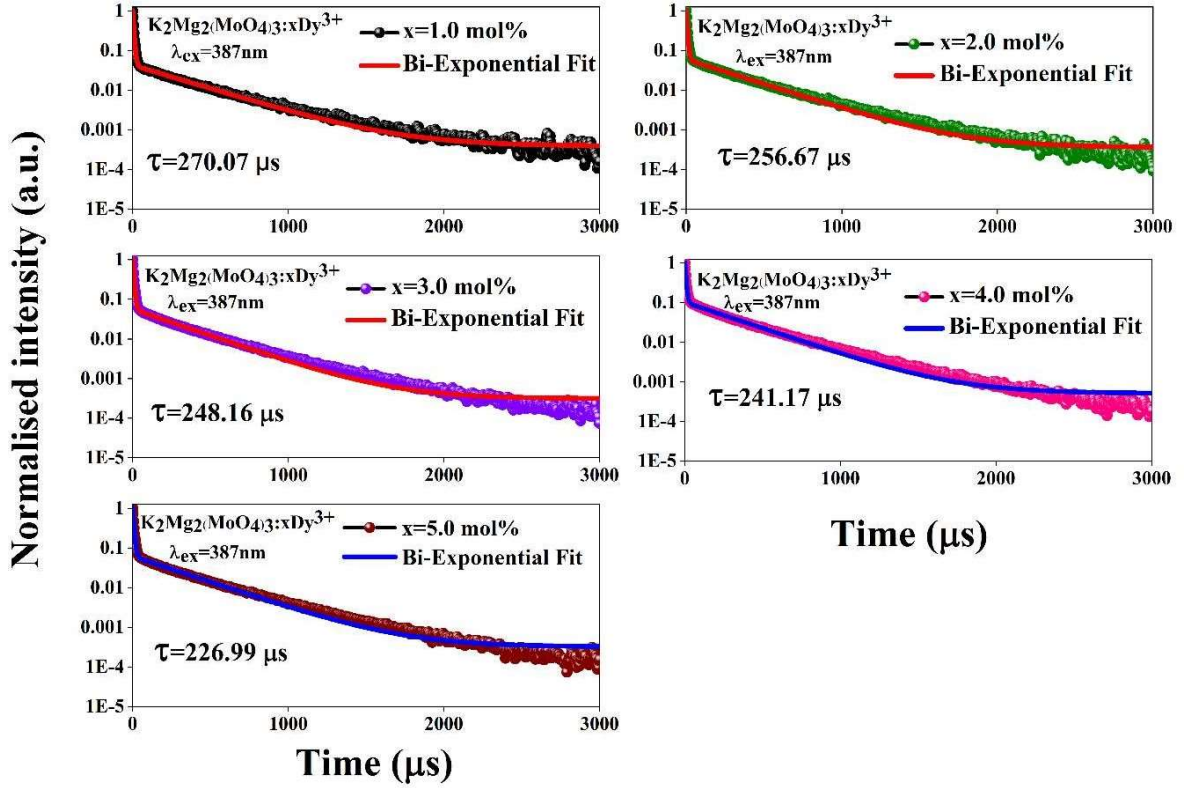


Fig.4.11. PL decay profile of $K_2Mg_2(MoO_4)_3: x Dy^{3+}$ ($0.0 \leq x \leq 5.0$, $\Delta x = 1.0$ mol %), phosphors under 387nm excitation.

Using the equation provided below, Auzel's model was able to further investigate the decrease in lifetime values with an increase in the concentration of Dy^{3+} ions.

$$\tau = \frac{c_0}{1 + \frac{c}{c_0} e^{-N/3}} \quad (4.13)$$

where N is the number of phonons produced during the relaxation, c is the concentration of Dy^{3+} ions, τ_0 is the intrinsic radiative lifetime, and τ is the estimated lifetime. Auzel's model fits the Dy^{3+} decay lifetime in KMM phosphor rather well, as shown in Fig. 4.12, and the fitting yields a value of τ_0 of 279.09 μs .

Using the intrinsic lifetime value, the luminous efficiency (η) is calculated as follows.

$$\eta = \frac{c}{c_0} = \frac{A_R}{A_R + A_{nR}} \quad (4.14)$$

$$\frac{1}{\eta} = \frac{1}{c/c_0} + A \quad (4.15)$$

$c \quad c_0 \quad nR$

Here, A_{nr} and A_r stand for the rates of relaxation by radiative and non-radiative mechanisms, respectively. Table 4.2 displays the luminous efficacy values (%), non-radiative rates (s^{-1}) and decay lifetime (μs).

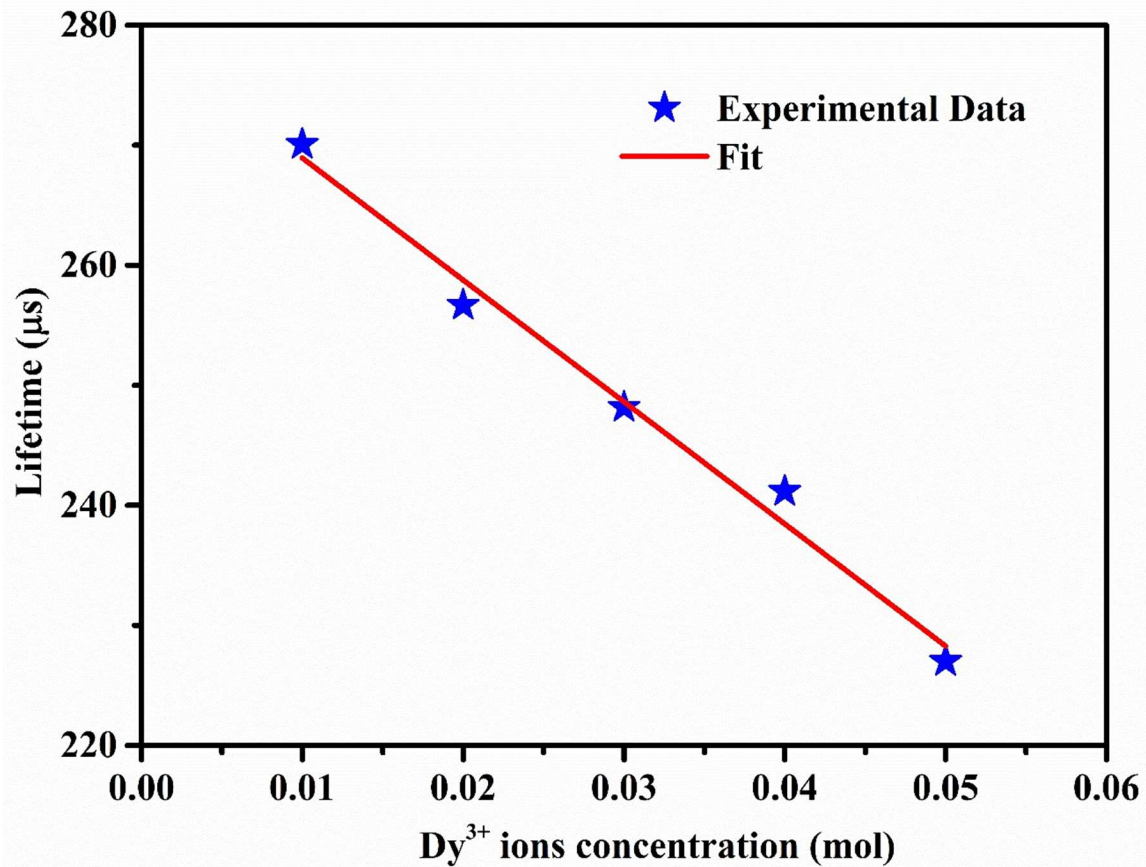


Fig.4.12. Dependence of photoluminescence decay lifetime on the Dy^{3+} doping concentration based on Auzel's model.

Table 4.2: KMM: $x Dy^{3+}$ ($x = 1.0, 2.0, 4.0,$ and 5.0 mol%) phosphors photoluminescence decay duration, non-radiative rate, and luminous effectiveness.

Sample ID KMM: $x Dy^{3+}$	Decay Lifetime (μs)	Nonradiative rate (s^{-1})	Quantum Efficiency (%)
$x = 1.0$ mol%	270.069	119.68	96.77
$x = 2.0$ mol%	256.67	312.98	91.97

x = 3.0mol%	248.16	446.54	88.92
x = 4.0mol%	241.17	563.38	86.41
x = 5.0mol%	226.99	822.25	81.34

CHAPTER 5: CONCLUSIONS

In conclusion, a solid-state approach was used to synthesis KMM:xDy^{3+} ($1.0 \leq x \leq 5.0$, $\Delta x = 1.0$ mol %). To understand their utilization in w-LEDs, the phase purity, crystal structure, morphology, and PL spectra of prepared phosphors were investigated. The orthorhombic configuration of the produced sample with space group $P2_12_12_1$ is confirmed by the XRD pattern. Using the Debye-Scherrer formula. The average size for all crystallites was found to be 30.53 nm. Particle sizes in morphological investigation range from 2 to 6 μm . The FTIR spectrum analysis verified that the structure's vibrational bands exist. Tauc plots were used to derive the band gap value, which for all phosphors varies from 5.45 to 5.55 eV based on the DRS data. KMM:Dy^{3+} exhibits five emission bands, the most intense is at 576 nm, following the transition from the $^4F_{9/2}$ ground state to the $^6H_{13/2}$ excited state, according to the results of the PL study. After applying Dexter theory to the PL data, it was determined that the dopant ion interaction was dipole-dipole in nature. All of the lifetime τ_{exp} values fall within the range of μs . It was found that the values of τ_{exp} dropped as the concentration of Dy^{3+} ions rose. As synthesised phosphor's CIE chromaticity coordinates are located in the yellowish white area. We would like to suggest KMM:Dy^{3+} phosphor as a viable option for use in white LED and other photonic device applications based on our examination of the aforementioned results because of its superior luminous efficiency, phase purity, and improved solubility for RE^{3+} ions.

CHAPTER 6: SCOPE OF FUTURE WORK

Literature survey on the topic area will be carried out. Optimization of synthesis methods. Optimization of activator/sensitizer concentration in the optimized methods. To enhance the emission intensity by varying the excitation wavelength, doping concentration, and by co-doping various activators/sensitizers ions. To increase this phosphor's usefulness for photonic applications such as display systems.

Dysprosium (Dy^{3+}) doping into KMM host material has been the focus of the current study, yielding an efficient and superior phosphor that may be employed in inexpensive phosphor-converted white light-emitting diodes (pc-w-LEDs). First off, co-doping these phosphors with other appropriate rare-earth ions (RE) like lutetium (Lu^{3+}), samarium (Sm^{3+}), yttrium (Y^{3+}), gadolinium (Gd^{3+}), terbium (Tb^{3+}), and others might improve their luminous qualities. This is because a new generation of quantum-integrated photonic devices may be made possible by RE ions co-doped in particular host matrix areas.

The current phosphor was created using a traditional solid-state reaction method, and its structural and photoluminescence characteristics have been described. To enhance the particle shape and decrease the particle size, a different synthesis technique like the sol-gel approach might be investigated. Using nitrates as metal precursors, the sol-gel combustion technique combines the sol-gel and combustion processes. In the Sol-gel method, the metal oxides that are produced undergo a number of reactions. The metal hydroxide solution is condensed to produce gels after the metal nitrate is quickly hydrolyzed, and xerogel is formed during the evaporation process and is subsequently burned at a high temperature. The final product is a fluffy, black structure that is sintered at different temperatures. This approach might

REFERENCES:

- [1] Y. Zhou, J. Lin, M. Yu, S. Wang, Comparative study on the luminescent properties of $Y_3Al_5O_{12}: RE^{3+}$ (RE: Eu, Dy) phosphors synthesized by three methods, *J. Alloys Compd.* 375 (2004) 93–97. <https://doi.org/10.1016/j.jallcom.2003.10.057>.
- [2] S. Kumari, A.S. Rao, R.K. Sinha, Structural and photoluminescence properties of Sm^{3+} ions doped strontium yttrium tungstate phosphors for reddish-orange photonic device applications, *Mater. Res. Bull.* 167 (2023). <https://doi.org/10.1016/j.materresbull.2023.112419>.
- [3] S.K. Jaganathan, A. John peter, Synthesis and luminescence properties of $CaGd_2(MoO_4)_4:Ln^{3+}$ (Ln = Eu^{3+} , Tb^{3+} , Dy^{3+} and Sm^{3+}) phosphors, *J. Lumin.* 199 (2018) 53–59. <https://doi.org/10.1016/j.jlumin.2018.03.013>.
- [4] G. Ouertani, M. Ferhi, K. Horchani-Naifer, M. Ferid, Effect of Sm^{3+} concentration and excitation wavelength on spectroscopic properties of $GdPO_4:Sm^{3+}$ phosphor, *J. Alloys Compd.* 885 (2021) 161178. <https://doi.org/10.1016/j.jallcom.2021.161178>.
- [5] P. Muralimanohar, G. Srilatha, K. Sathyamoorthy, P. Vinothkumar, M. Mohapatra, P. Murugasen, Preparation and luminescence properties of Dy^{3+} doped $BaAlBO_3F_2$ glass ceramic phosphor for solid state white LEDs, *Optik (Stuttg)*. 225 (2021) 165807. <https://doi.org/10.1016/j.ijleo.2020.165807>.
- [6] P. Rohilla, A.S. Rao, Synthesis optimisation and efficiency enhancement in Eu^{3+} doped barium molybdenum titanate phosphors for w-LED applications, *Mater. Res. Bull.* 150 (2022) 111753. <https://doi.org/10.1016/j.materresbull.2022.111753>.
- [7] M. He, Q. Bian, Z. Zhang, B. Dong, G. Zhu, R. Xue, Y. Cong, K. Liu, Luminescent properties of novel $K_2Mg_{2-x}(MoO_4)_3:xEu^{3+}$ red light-emitting phosphor, *Mater. Today Commun.* 33 (2022) 104538. <https://doi.org/10.1016/j.mtcomm.2022.104538>.
- [8] J. Xie, X. Zhang, L. Cheng, H. Tang, X. Yu, Y. Wang, Z. Wang, X. Mi, Q. Liu, Photoluminescence properties of novel $K_2Mg_2(MoO_4)_3:Sm^{3+}$ orange-red emitting phosphors for white light emitting diodes, *Opt. Mater. (Amst)*. 107 (2020) 110008. <https://doi.org/10.1016/j.optmat.2020.110008>.
- [9] W.T. Carnall, P.R. Fields, K. Rajnak, Electronic energy levels of the trivalent lanthanide aquo

- ions. IV. Eu^{8+} , J. Chem. Phys. 49 (1968) 4424–4442. <https://doi.org/10.1063/1.1669893>.
- [10] W.T. Carnall, P.R. Fields, K. Rajnak, Electronic Energy Levels of the Trivalent Lanthanide Aquo Ions. III. Tb^{3+} , J. Chem. Phys. 49 (1968) 4447–4449. <https://doi.org/10.1063/1.1669895>.
- [11] W.T. Carnall, P.R. Fields, K. Rajnak, Electronic Energy Levels of the Trivalent Lanthanide Aquo Ions. IV. Eu^{3+} , J. Chem. Phys. 49 (1968) 4450–4455. <https://doi.org/10.1063/1.1669896>.
- [12] S. Kumari, Anu, A. Prasad, P. Rohilla, A.S. Rao, Prospective applications of thermally stable Dy^{3+} doped potassium zinc strontium borate (KZSB) glasses in w-LEDs, J. Mater. Sci. Mater. Electron. 34 (2023). <https://doi.org/10.1007/s10854-023-10272-6>.
- [13] S. Kumari, A.S. Rao, R.K. Sinha, Investigations on photoluminescence and energy transfer studies of Sm^{3+} and Eu^{3+} ions doped $\text{Sr}_9\text{Y}_2\text{W}_4\text{O}_{24}$ red emitting phosphors with high color purity for w-LEDs, J. Mol. Struct. 1295 (2024) 136507. <https://doi.org/10.1016/j.molstruc.2023.136507>.
- [14] J. Zhong, X. Chen, D. Chen, M. Liu, Y. Zhu, X. Li, Z. Ji, A novel rare-earth free red-emitting $\text{Li}_3\text{Mg}_2\text{SbO}_6:\text{Mn}^{4+}$ phosphor-in-glass for warm w-LEDs: Synthesis, structure, and luminescence properties, J. Alloys Compd. 773 (2019) 413–422. <https://doi.org/10.1016/j.jallcom.2018.09.162>.
- [15] G. V. Lokeswara Reddy, L. Rama Moorthy, B.C. Jamalaih, T. Sasikala, Preparation, structural and luminescent properties of $\text{YAl}_3(\text{BO}_3)_4:\text{Dy}^{3+}$ phosphor for white light-emission under UV excitation, Ceram. Int. 39 (2013) 2675–2682. <https://doi.org/10.1016/j.ceramint.2012.09.034>.
- [16] V. Chornii, V. Boyko, S.G. Nedilko, K. Terebilenko, M. Slobodyanik, Synthesis, Morphology and Luminescence Properties of Pr^{3+} -containing Phosphate-Molybdate Glass-Ceramics, Proc. 2021 IEEE 11th Int. Conf. "Nanomaterials Appl. Prop. N. 2021 (2021) 1–4. <https://doi.org/10.1109/NAP51885.2021.9568601>.
- [17] W. Wang, X. Yang, S. Xiao, $\text{Ba}_3\text{Y}_2\text{WO}_9:\text{Mn}^{4+}$: A near-UV and yellow-green light excited red phosphor for greenhouse cultivation, J. Lumin. 225 (2020) 117406. <https://doi.org/10.1016/j.jlumin.2020.117406>.

- [18] M. Ye, G. Zhou, L. Zhou, D. Lu, Y. Li, X. Xiong, K. Yang, M. Chen, Y. Pan, P. Wu, Z. Wang, H. Liu, Q. Xia, Luminescent properties and energy transfer process of Sm^{3+} - Eu^{3+} co-doped $\text{MY}_2(\text{MoO}_4)_4$ (M=Ca, Sr and Ba) red-emitting phosphors, *Solid State Sci.* 59 (2016) 44–51. <https://doi.org/10.1016/j.solidstatesciences.2016.07.005>.
- [19] S. Chen, Y. Wang, B. Zhao, B. Deng, Y. Liu, S. Chen, J. Wang, G. Wang, R. Yu, Luminescence properties of novel orange-red-emitting $\text{Gd}_2\text{InSbO}_7:\text{Sm}^{3+}$ phosphor with high color purity for W-LEDs, *J. Lumin.* 237 (2021) 118148. <https://doi.org/10.1016/j.jlumin.2021.118148>.
- [20] H. Zhu, M. Fang, Z. Huang, Y. Liu, K. Chen, X. Min, Y. Mao, M. Wang, Photoluminescence properties of $\text{Li}_2\text{Mg}_2(\text{WO}_4)_3:\text{Eu}^{3+}$ red phosphor with high color purity for white LEDs applications, *J. Lumin.* 172 (2016) 180–184. <https://doi.org/10.1016/j.jlumin.2015.12.021>.
- [21] K.V. Raju, C.N. Raju, S. Sailaja, S.J. Dhoble, B.S. Reddy, Emission analysis of Sm^{3+} and Dy^{3+} : $\text{Ba}_3\text{Y}_2\text{WO}_9$ ceramics, *J. Lumin.* 134 (2013) 297–302. <https://doi.org/10.1016/j.jlumin.2012.08.030>.
- [22] J. Tang, J. Si, X. Fan, Y. Liu, G. Li, G. Cai, Tunable emission, energy transfer and thermal stability of Ce^{3+} , Tb^{3+} co-doped $\text{Na}_2\text{BaCa}(\text{PO}_4)_2$ phosphors, *J. Rare Earths* 40 (2022) 878–887. <https://doi.org/10.1016/j.jre.2021.05.016>.
- [23] S. Kaur, A.S. Rao, M. Jayasimhadri, Spectroscopic and photoluminescence characteristics of Sm^{3+} doped calcium aluminozincate phosphor for applications in w-LED, *Ceram. Int.* 43 (2017) 7401–7407. <https://doi.org/10.1016/j.ceramint.2017.02.129>.

PLAGIARISM REPORT

Similarity Report

PAPER NAME

2 editable sem 4 dissertation.docx

WORD COUNT

5953 Words

CHARACTER COUNT

33506 Characters

PAGE COUNT

20 Pages

FILE SIZE

65.3KB

SUBMISSION DATE

Jun 5, 2024 2:17 PM GMT+5:30

REPORT DATE

Jun 5, 2024 2:17 PM GMT+5:30

● 10% Overall Similarity

The combined total of all matches, including overlapping sources, for each database.

- 3% Internet database
- 5% Publications database
- Crossref database
- Crossref Posted Content database
- 6% Submitted Works database

● Excluded from Similarity Report

- Bibliographic material
- Quoted material
- Cited material
- Small Matches (Less than 10 words)

ACCEPTANCE PROOF

From: **EquinOCS** <equinocs-admins@springernature.com>
Date: Thu, May 30, 2024 at 9:21 AM
Subject: Accepted paper in the EquinOCS system
To: Allam Rao <drsallam@gmail.com>

This message has been sent by the EquinOCS system
<https://equinocs.springernature.com/>

PLEASE DO NOT REPLY

=====

Dear Allam Rao,

We are pleased to inform you that your paper

002: "Photo-luminescent studies of molybdate phosphor doped with Dy³⁺ ions for w-LEDs"

has been accepted for

International Conference on Atomic, Molecular, Material, Nano, and Optical Physics with Applications (ICAMNOP-2023)

Please find the reports beneath.

REPORT

Modified the manuscript as per the reviewer's comments

REPORT

The paper has been accepted for publication.



**International Conference on Atomic, Molecular, Material,
Nano and Optical Physics with Applications
(ICAMNOP-2023)**

Organized by: Department of Applied Physics,
Delhi Technological University Delhi-110042, India
December 20th-22nd, 2023



PAYMENT RECEIPT

BILL TO

Ms. Yashika Saraswat
8814089693
yashikasaraswat2001@gmail.com

RECEIPT NO.

126/231123195052

AMOUNT

4885.20INR

DATETIME

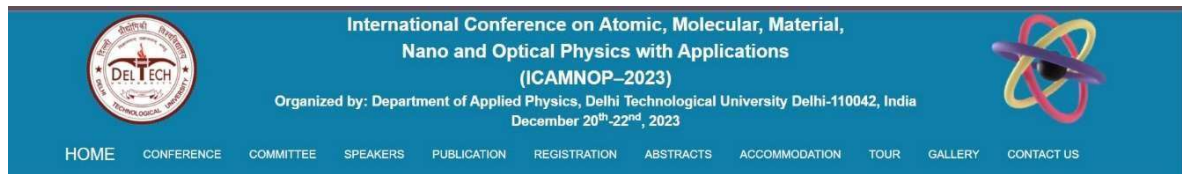
23-11-2023 19:53:35

PAYMEN DETAILS	
Transaction Id	: 126/231123195052
Payment Method	: Credit/Debit Card
Payment Gatway	: Stripe Payment Gatway

Note:

* This is a computer generated receipt and no signature is required.

SCOPUS INDEXING PROOF



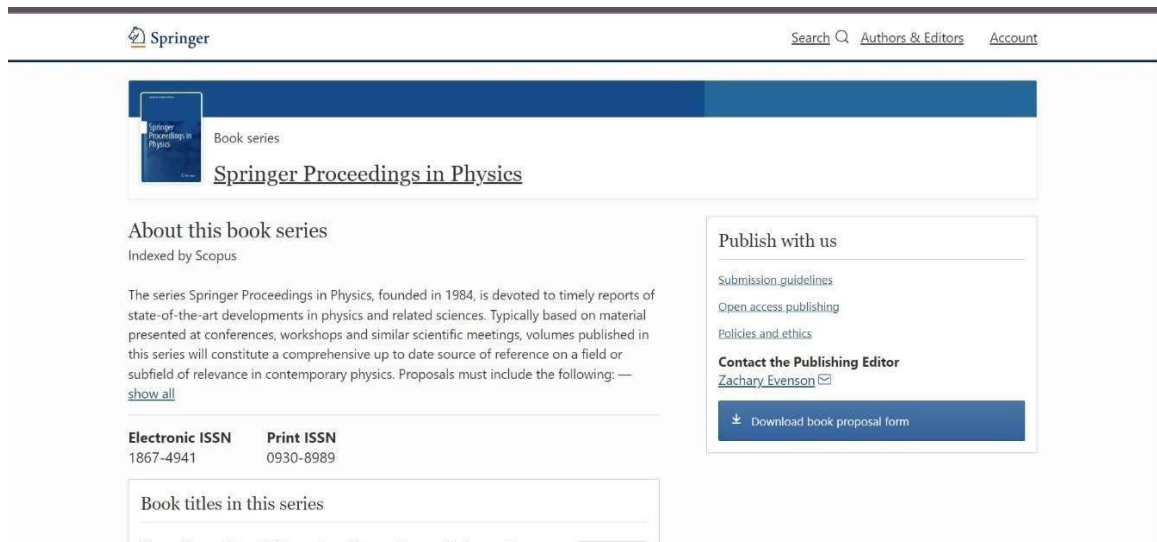
International Conference on Atomic, Molecular, Material,
Nano and Optical Physics with Applications
(ICAMNOP-2023)
Organized by: Department of Applied Physics, Delhi Technological University Delhi-110042, India
December 20th-22nd, 2023

HOME CONFERENCE COMMITTEE SPEAKERS PUBLICATION REGISTRATION ABSTRACTS ACCOMMODATION TOUR GALLERY CONTACT US

Login

About The Conference

The International Conference on Atomic, Molecular, Material, Nano and Optical Physics with Applications (ICAMNOP 2023) will focus on developments in atomic, molecular, material, Nano and Optical Physics which have proved to be powerful science supporting many other areas of science & technology, including industrial, information, energy, global Change, defense, health and medical environmental, space and transportation technology. The conference will involve experimental and theoretical studies of atoms, ions, molecules and nanostructures both at the fundamental level & on the application side using advanced technology. Using modern tools of high – field and ultra-fast physics, one no longer merely observes nature, but can reshape and redirect atoms, molecules, particles or radiation. This new drive towards harnessing quantum dynamics is enormously important to future developments in fundamentals physics and applied energy science. Third generation synchrotron sources offer new opportunities to study radiation – matter interactions. Optical techniques have also played a very important role in the creation, understanding and manipulation of atomic and molecular Bose- Einstein Condensates. Complete quantum mechanical description of such properties and interactions is required and to this end, the present conference aims at bringing together experimental and theoretical scientists working in various fields of "Atomic, Molecular, Material, Nano and Optical Physics", to share and exchange new ideas. Topics of interest in the conference include: Atomic & Molecular Structure, Collision Process, clusters, surfaces and exotic particles and Applications, Laser cooling, trapping and Bose – Einstein condensation, High precision and Ultracold phenomena, High harmonic generation and applications, Coherent optical phenomena, Ultrafast dynamics at the Femto- or Atto second scale, ion – include radiation damage in particular of biomolecules, atomic spectroscopy and molecular physics of antimatter, free electron laser, particle acceleration generated by high – power laser, Quantum optics and its application to Mesoscopic system. Other topics covered are: Spectroscopy of Solar and Stellar Plasma, The atomic universe: Spectra as Probes of Cool Gas. The rapidly growing field of nanophysics is introduced as a separate conference topic this time, which include, Nano-structures and Photonics. In the last, a session will also be devoted to application of Atomic, Molecular Optical and Nano Physics in Petroleum, Renewable energy, Environmental Science, Information Technology, Health and Education in Developing Countries.



Springer Search Authors & Editors Account

Book series
Springer Proceedings in Physics

About this book series
Indexed by Scopus

The series Springer Proceedings in Physics, founded in 1984, is devoted to timely reports of state-of-the-art developments in physics and related sciences. Typically based on material presented at conferences, workshops and similar scientific meetings, volumes published in this series will constitute a comprehensive up to date source of reference on a field or subfield of relevance in contemporary physics. Proposals must include the following: — [show all](#)

Electronic ISSN 1867-4941 Print ISSN 0930-8989

Book titles in this series

Publish with us

- [Submission guidelines](#)
- [Open access publishing](#)
- [Policies and ethics](#)

Contact the Publishing Editor
[Zachary Evenson](#)

Download book proposal form